LEBANESE AMERICAN UNIVERSITY

Behavior of Un-reinforced Concrete Masonry Infill Walls under Lateral Earthquake Loads

By

Ziad Charbel Azzi

A thesis submitted in partial fulfillment of the requirements

For the degree of Master of Science in Civil and Environmental Engineering

School of Engineering

December 2016

LAU
الجامعة اللبنانية الأميركية
Lebanese American University

Lebanese American University

School of Engineering ; Byblos Campus

THESIS APPROVAL FORM

Student Name: Ziad Azzi I.D. #: 200803405

Thesis Title : Behavior of Un-reinforced Concrete Masonry Infill Walls under Lateral Earthquake Loads

Program: Master of Science in Civil and Environmental Engineering

Department: Civil Engineering

School: Engineering

The undersigned certify that they have examined the final electronic copy of this thesis and approved it in Partial Fulfillment of the requirements for the degree of:

Master of Science in the major of Civil and Environmental Engineering

Thesis Advisor's Name Caesar Abi Shdid Signature [redacted] Date 19/12/2016

Committee Member's Name MAZEN TASSABA Signature [redacted] Date 19/12/2016

Committee Member's Name Camille Issa Signature [redacted] Date 19/12/2016

LAU
الجامعة اللبنانية الأميركية
Lebanese American University

THESIS COPYRIGHT RELEASE FORM

LEBANESE AMERICAN UNIVERSITY NON-EXCLUSIVE DISTRIBUTION LICENSE

By signing and submitting this license, you (the author(s) or copyright owner) grants to Lebanese American University (LAU) the non-exclusive right to reproduce, translate (as defined below), and/or distribute your submission (including the abstract) worldwide in print and electronic format and in any medium, including but not limited to audio or video. You agree that LAU may, without changing the content, translate the submission to any medium or format for the purpose of preservation. You also agree that LAU may keep more than one copy of this submission for purposes of security, backup and preservation. You represent that the submission is your original work, and that you have the right to grant the rights contained in this license. You also represent that your submission does not, to the best of your knowledge, infringe upon anyone's copyright. If the submission contains material for which you do not hold copyright, you represent that you have obtained the unrestricted permission of the copyright owner to grant LAU the rights required by this license, and that such third-party owned material is clearly identified and acknowledged within the text or content of the submission. IF THE SUBMISSION IS BASED UPON WORK THAT HAS BEEN SPONSORED OR SUPPORTED BY AN AGENCY OR ORGANIZATION OTHER THAN LAU, YOU REPRESENT THAT YOU HAVE FULFILLED ANY RIGHT OF REVIEW OR OTHER OBLIGATIONS REQUIRED BY SUCH CONTRACT OR AGREEMENT. LAU will clearly identify your name(s) as the author(s) or owner(s) of the submission, and will not make any alteration, other than as allowed by this license, to your submission.

Name: Ziad [redacted]

Signature:

Date: December 16, 2016

LAU
الجامعة اللبنانية الأميركية
Lebanese American University

PLAGIARISM POLICY COMPLIANCE STATEMENT

I certify that:

- I have read and understood LAU's Plagiarism Policy.
- I understand that failure to comply with this Policy can lead to academic and disciplinary actions against me.
- This work is substantially my own, and to the extent that any part of this work is not my own I have indicated that by acknowledging its sources.

Name: Ziad [redacted]

Signature: [redacted]

Date: Decer [redacted]

Dedication

To my special and beloved family

Acknowledgments

I wish to start by thanking and praising my thesis advisor, Dr. Caesar Abi Shdid, for his massive support, dedication, commitment and guidance during the three years spent on this research. This research would not have been possible without his effort.

I would also like to thank the other members of the committee, Dr. Camille Issa and Dr. Mazen Tabbara, along with Dr. Gebran Karam for their continuous guidance and availability for advice whenever I knocked on their doors on campus.

I wish to express my gratitude to my parents and siblings for their continuous support and motivation to always aim for my ambitions and dreams.

Special thanks go to the laboratory supervisor, Mr. Georges Chaccour, for his monumental effort and time spent, helping me in the tiniest details in order to make this work as accurate as possible. Finally, I would also like to show appreciation and thank my mechanical engineering colleagues Mr. Christian Adib and Mr. Jean-Pierre Chebat for their help and support in the coding.

Behavior of Un-reinforced Concrete Masonry Infill Walls under Lateral Earthquake Loads

Ziad Charbel Azzi

Abstract

Reinforced concrete buildings with unreinforced masonry infill walls constitute the majority of new and old building inventories in the Middle East. In the absence of mandatory earthquake design requirements, such buildings may be susceptible to costly and life-threatening damage caused by high seismic activity. The location of Lebanon on the intersection of two highly active tectonic plates, serves only to exacerbate this issue; making the investigation of the behavior of such walls under seismic loading an urgent affair.

This research summarizes past findings and commonly accepted theories on the behavior of such infills, and outlines limitations of existing work. Shake table experimental testing is utilized on 3:10 scaled specimens of a single story reinforced concrete frame with a masonry infill wall in between. The frame is designed and constructed with local materials and according to commonly used construction practices in the region. The specimens are instrumented and tested with simulated out-of-plane ground motion of the 1940 El Centro earthquake Displacement and strain data is recorded and compared with a computer model of the frame modeled using a finite element analysis software. Comparisons are also made between the observed overall behavior and that predicted by the computer model. While the specimens recorded strains in the mortar joints exceeding cracking limits, the overall out-of-plane stability of the wall in out of plane bending was maintained and no collapse of the infill was recorded. Findings are formulated into recommendations and conclusions are made concerning the use of such structural elements in widespread building construction.

Keywords: Reinforced concrete buildings, Unreinforced masonry infill walls, Finite element, Shake table, Instrumentation, Analytical model.

Table of Contents

List of Tables

Table of Figures

Chapter One
Introduction

In most countries, unreinforced masonry buildings make up a large portion of the existing buildings inventory and a dominant and common form of construction [1]. In developing countries, such structures are designed and built without reference to any particular code practices or engineering principles [2]. This renders unreinforced masonry building extremely vulnerable to lateral, mainly seismic, loads. In addition, many characteristics of the behavior of unreinforced masonry walls and buildings under such loads remain to be understood by researchers. This task is made complex by factors such as diversity of construction methods and skills, non-standard design practices, regional differences in construction materials, and the age of existing buildings. Of particular interest to this research is the effect of seismic loads on masonry infill walls. The fact that these walls are unreinforced and loosely attached to the surrounding frame makes them specifically vulnerable to out-of-plane bending moments produced by lateral loads. While their failure may or may not cause the failure of the entire building, depending on how much their presence increases the lateral stiffness of the structure, such failure can present a significant hazard on the lives of building inhabitants and passersby.

Buildings with reinforced concrete moment resisting frames and unreinforced masonry infill walls are the most common type of construction used for low- and mid-rise buildings in developing countries [2]. Some developing countries in the Near East region, namely Lebanon, Syria and Jordan are split by the Yammouneh fault that separates the Arabian plate from the African plate. In this specific location, these plates move parallel to each other but in opposite direction, making this type of fault a transform fault. According to the universal building code, IBC 2015, the above mentioned countries are located in seismic zone 2B, where the maximum peak ground acceleration for seismic activities in the region can reach up to 0.2g. This translates to earthquakes that can reach magnitudes of up to 7.0 on the Richter scale. Such high levels

of seismic loads will create large out-of-plane bending moments that result in rather high flexural stresses at the bases of infill walls. This, coupled with lack of a positive wall anchorage to the structure, will render the commonly-constructed buildings, with unreinforced masonry infills, highly vulnerable to the explosive failure of these walls.

This study utilizes shake table experimental testing of a scaled model of such typical buildings with reinforced concrete frame and unreinforced masonry infill walls, to better understand their behavior and failure mechanisms under seismic loads. A non-linear time history analysis of the frame is performed on a finite element analysis software SAP2000 [3] and the results are compared. Conclusions are formulated and recommendations are suggested to the design and construction methods that would improve the resistance of buildings in this particular geographic region to earthquake hazards.

Chapter Two
Literature Review

In the past two decades, a rather large number of studies was conducted and published on the subject of the dynamic behavior of infilled frames due to earthquake loading. This increase of interest in this subject matter can be attributed to several reasons; one such reason is the widespread construction of unreinforced masonry buildings in the last century and the need to develop a general procedure to evaluate the extent of the damage suffered by unreinforced masonry walls. Other reasons include the need to investigate whether masonry infills can increase the lateral stiffness and lateral load capacity of the structure if they are considered to interact with their neighboring frames. This increase in studies on this subject has not however been without difficulties. What makes research on this topic difficult is that the structure's behavior under dynamic loading is largely related to the construction method and materials used, as well as the qualifications of the masons. Moreover, the dynamic testing associated with scaled models has always been a cause of concern due to the scaled material properties and the limitation placed on the specimen size by the load capacity of available shake tables. Completed and published studies on this topic can be grouped in two main categories. On one hand, there are the studies related to developing standard procedures to evaluate existing unreinforced masonry buildings, and on the other hand, there are the experimental studies related to determining the advantages of considering masonry infill frames to interact with their respective frames and contribute to the lateral stiffness of the structure.

Awareness regarding the problem of unreinforced masonry buildings was raised due to the devastating effects that the North American earthquakes [4] had on these types of buildings. Since there was no clear procedure to follow when investigating old masonry buildings or designing new ones according to seismic regulations, engineers largely resorted to various conservative approaches [4]. By the end of 1933, many cities in the USA had already banned the construction of unreinforced masonry buildings [4].

Eventually, research evolved to develop and improve new structural systems constructed with reinforced masonry. This new type of buildings was more ductile and offered much more seismic resistance. However, nothing was done to improve the understanding of the seismic behavior of unreinforced masonry construction especially that most of the cities were left with a large inventory of unreinforced masonry (URM) buildings.

As with other types of construction, the particular structural characteristics and layout of an unreinforced masonry building are the main variables affecting its earthquake survival or failure. To be effective, a seismic evaluation must assess all possible modes of failure found in unreinforced masonry structures. Recognized modes include: lack of anchorage, anchor failure, in-plane failures, out-of-plane failures, combined in-plane and out-of-plane effects, and diaphragm-related failures [4]. Bruneau [5] reported on the practical applications and theoretical background of a new procedure named the *ABK method* to evaluate unreinforced masonry buildings, which had been recently integrated into the new Canadian Guidelines [6] following development in California. The *ABK method* addresses all of the above modes of failure and draws a relationship between the quality of construction and materials used and peak ground acceleration on the one hand and structural damage on the other hand. One of the concepts endorsed by the methodology is that walls are infinitely rigid in-plane. Also, by imposing limits on diaphragms spans, the methodology aims at increasing out-of-plane stability and structural integrity.

By testing three walls of three-wythe common bricks, five walls of clay blocks, and twelve walls of concrete blocks with different height to thickness ratios, it was concluded that unreinforced masonry buildings are most vulnerable to out-of-plane failure [5]. Furthermore, it was also formulated that proper anchorage to floors and roof diaphragms increases resistance to more severe earthquakes. The study presented a numerical example to illustrate the applicability of the proposed method. The example consisted of a two-story building with a 9x29 meters plan dimension. The demonstrative building had unreinforced clay masonry load-bearing exterior walls with varying thicknesses of two or three wythes. The building as such could be analyzed using the *ABK method* since it met the special conditions required for the use of this special

procedure. The numerical example was developed for the most severe seismic zone that could be encountered in Canada. It was concluded that there are several energy dissipation mechanisms that can help alleviate the problem of masonry being such a brittle material incapable of inelastic straining [5]. Buildings not meeting the requirements for the use of the *ABK method* can be analyzed using dynamic analysis or finite element analysis. Since it has not received any endorsement yet, the special procedure's use has remained voluntary.

Given that all URM buildings were designed and constructed in the absence of mandatory earthquake-design requirements, they are unquestionably the type of construction most vulnerable to earthquakes. In that respect, there needs to be a realistic approach to assess the structural capacity and earthquake resistance of the components of an unreinforced masonry building. However, in order to do that, the multiple and diverse modes of failure of buildings subjected to earthquake excitation should be understood. Bruneau [4] summarized the seismic hazards in existing URM buildings and their general modes of failure.

One such mode of failure is the lack of proper anchorage. In most unreinforced masonry buildings, there exists a total absence of positive anchorage of the diaphragms to the unreinforced masonry walls. This resting of one structural component on another creates a simple support, unable to cope with rotational displacement or the transfer of moments. In the absence of these anchors, the exterior walls behave as very long cantilevers with a length that of the total building height. This scenario increases the vulnerability of the unreinforced masonry walls to out-of-plane failure due to excessive flexural stresses at their bases, in addition to global structural failure caused by the slippage of beams and joists from their respective supports [4].

Another mode of failure in URM buildings is the anchor failure characterized by the failure of the metal of the anchor itself or by its rupture at the connection points. A third mode of failure elaborated by Bruneau [4] is the in-plane failures of unreinforced masonry walls caused by excessive bending or shear. This type of failure is manifested by double-diagonal shear cracking forming an X mark. The out-of-plane mode of failure

represents the mode of failure that URM buildings are most vulnerable to. While joist-to-wall anchors provide some out-of-plane support to the walls, any failure in these types of anchors jeopardizes the safety of the building. It was also noted by Bruneau [4] that the in-plane failures do not endanger the load carrying capacity of a wall as much as the explosive and unstable out-of-plane ones. Since earthquakes forces are bidirectional in nature, walls might fail by a combination of in-plane and out-of-plane effects. The more in-plane shear cracking occurs, the more out-of-plane stability of the wall is lost. Diaphragm-related failures were also mentioned as a possible mode of failure. Since flexible floor diaphragms behave as deep beams spanning between unreinforced masonry walls, the rotation at its ends can induce damage at the walls' corners. The absence of a good shear transfer between reaction walls and diaphragms can also damage the corners of the walls [4].

Since earthquakes dynamically excite buildings, displacements are in most cases not linearly related to forces. Because of this nonlinear behavior, it is not always appropriate to use simple static and linear analysis to evaluate existing unreinforced masonry buildings or to design new ductile reinforced masonry walls and frames. Abrams and Costley [7] presented an overview of existing analysis methods for the seismic evaluation of unreinforced masonry buildings. The study tested whether these analysis methods can be used to estimate true nonlinear dynamic response of existing unreinforced masonry buildings. Four analytical models were evaluated: linear static analysis, linear dynamic analysis, non-linear static analysis, and non-linear dynamic analysis. In the linear static analysis method, an approximate base shear is estimated for the whole building and lateral forces are distributed to each floor. In the linear dynamic analysis method, the shape of the vibration of the building is inspected to determine the effective modal weight to be used instead of the total weight of the building used in linear static analysis. In addition, the differential amplification of base accelerations for the diaphragms and shear walls is only revealed by using the dynamic analysis approach [7].

The nonlinear static analysis procedure allows the modeling of the softening of the overall system as beams, columns and bracing members become plastic. It was also the

suggested method for the evaluation of unreinforced masonry buildings under a set of guidelines for systems using all types of construction materials. However, a computer model of a test structure showed that the push-over curves did not agree well with measured force-deflection curves, and that diaphragm inertial forces took place non-concurrently with wall inertial forces because of their different frequencies. The study concluded that this method should only be used with the coefficient method or the capacity-spectrum to pinpoint the maximum target displacement a system is likely to encounter for a particular base motion [7]. The study found that a nonlinear dynamic analysis was necessary to represent the two distinctly different frequencies encountered in the walls and diaphragms, in addition to the representation of the flexible diaphragms and the post-cracking effects. A simple three-degree-of-freedom system was found to provide an accurate depiction of peak displacements and frequencies of the system with rocking behavior. The four analytical models were validated experimentally using two reduced scale, two-story brick buildings subjected to simulated earthquake motions on a shaking table. The two experimental building models were constructed with different opening sizes and locations to produce dissimilar stiffnesses and strengths for the shear walls. Each test structure was subjected to scaled-versions of the motions measured during the 1985 Nahanni earthquake in the NW Canadian territories. The tests showed that the linear static analysis, the linear dynamic analysis and the non-linear static analysis methods raise concerns due to being conservative or due to the structure not behaving as assumed. The study concluded that a non-linear dynamic analysis was needed [7].

Contrary to common practice, the presence of masonry infills largely influences the overall behavior of the structure when subjected to lateral forces. By considering that masonry infills interact with surrounding frames and diaphragms, the lateral stiffness and lateral capacity of the structure are significantly increased. However, this influence of infills on the overall behavior of the structure has been noticed to change with the direction of the loading. Guidelines for evaluating the strength and stiffness of unreinforced masonry infill panels for in-plane and out-of-plane loading were provided by Al Chaar [8]. The study proposed a multi-step procedure based on the use of non-

linear static analysis using the equivalent strut method, and validated the method using experimental and computational modeling using non-linear finite element analysis.

The transfer of lateral forces across infilled frames causes a non-uniform stress distribution within the infill and frame elements. The infill wall fails when either of its shear or compressive strength is reached. To capture the nonlinear behavior of all material components including masonry, mortar, concrete and steel, the lateral load capacity of the frame-infill systems was determined using a nonlinear finite elements model [8]. Predicting the in-plane strength of infilled frames is a complex and statically indeterminate problem since the strength of a composite system is not simply the summation of the infill properties plus those of the frame. During testing of infill specimens between two frames, diagonal cracks developed in the center of the panel and gaps were formed between the frame and the infill in the nonleaded diagonal corners of the specimen [8]. The study used this observation to develop the equivalent strut width in order to better model the behavior of the infills. The strut should be assigned strength parameters consistent with the properties of the infill it represents. The equivalent strut method developed can be used for fully infilled frames, partially infilled frames, and perforated panels with various modifications of each [8].

Regarding the in-plane stiffness evaluation of unreinforced masonry infills, the use of an equivalent strut in the non-linear static (pushover) analysis yields mathematical models which are more flexible than experimental ones. To accurately represent actual displacements, the initial stiffness of the wall must be increased and the displacement at ultimate load reduced. This adjustment of the pushover curve is accomplished with a bilinear load-deflection relationship curve that is defined by three points: the origin, the yield load and displacement point, and the ultimate load and displacement point [8]. This modification is shown to reasonably predict the initial stiffness, the ultimate load capacity, and the displacement at ultimate load for the infilled structures.

For out-of-plane evaluation of unreinforced masonry infills, the strength and stiffness components are normally combined. The resistance of out-of-plane lateral forces is accomplished by two mechanisms: the arching action developed after surface

cracking of the panels, and the masonry tensile strength up to initial cracking. The study suggests that perforated panels and existing infill damage be accounted for by using reduction factors [8]. The study also proposes that when analyzing the in-plane capacity of an infilled structure, the effects of the out-of-plane loading should be accounted for since it might significantly reduce the in-plane capacity. The experimental validation was conducted on 305x305 centimeters infill walls, including full infill, partial infill, and perforated infill between reinforced concrete frames. The study concluded that the pushover method gives reliable results when compared to experimental data and non-linear finite element analysis. The study suggests that in case that pushover analysis was not available, an engineer could resort to a linear static procedure considering some guidelines provided in the study. In addition, a non-linear dynamic analysis was not recommended due to the complexities involved with solving some problems that arise from the adoption of that method [8].

Since unreinforced masonry buildings constitute a big problem in terms of seismic behavior, several procedures have been developed over time for their assessment. Each procedure has its advantages and disadvantages in its formulation and the treatment of uncertainties that are always present when dealing with earthquake analysis. Restrepo-Velez and Magenes [9] presented a procedure for the seismic risk assessment of unreinforced masonry buildings, called MeBaSe. The proposed procedure is based on four features that include the seismic demand and structural capacity by means of displacement, the structural capacity and response in terms of concepts of mechanics, the consideration of in-plane and out-of-plane failure mechanisms, and the sources of uncertainty. For in-plane failure modes, the proposed procedure was developed from the idea of displacement-based approach for vulnerability evaluation of classes of buildings. It uses a single-degree-of-freedom (SDOF) simplification in modelling that accounts for the various displacement profiles according to the failure mechanism or displacement profile at a given limit state [9]. The study presents four possible displacement profiles for different limit states and in-plane failure modes. Each displacement profile can be linked to a typical situation for unreinforced masonry buildings.

By analyzing pushover results for a four-story masonry building, it is shown that the maximum lateral strength force is virtually the same for higher values of referential shear strength. For the simplified model for out-of-plane failure modes, the procedure is restricted to one-way bending. The MeBaSe procedure considers three sources of uncertainty with regard to seismic risk estimation: ground-motion demand, damage state threshold, and capacity response. A case study was conducted in Benevento, Italy that showed the feasibility of the methodology at an urban scale [9]. By introducing the procedure at urban scale, a key issue raised is the definition of building classes. As part of the case study, a survey was conducted to classify all unreinforced masonry buildings according to seismic classes. From these classes, several probability density functions were developed to estimate the probabilities of each unreinforced masonry building belonging to a certain seismic class.

Chiou et al. [10] investigated the structural behavior of a framed masonry wall subject to in-plane monotonic loading using full-scale experimental tests. Since the materials used in framed masonry construction are mostly brittle and the failure of these walls often starts from the cracking of the mortar and separation of the masonry units, the behavior is nonlinear and discontinuous. The cracking and separation phenomenon occurring in the masonry structures causes distinct block elements. This study discusses the use of discontinuous deformation (DDA) method to analyze the block system. Three full-scale structural frames measuring 320x300 cm were compared: a reinforced concrete (RC) frame with no masonry infill, a RC frame with a partially infilled masonry wall, and a RC frame with a complete masonry infill wall.

Using the DDA, the displacement and equilibrium equations were solved in the same way as the finite-element method. The method incorporated a complete block kinematic that satisfied the conditions of no tension and no interpenetration of blocks at any time. Contact springs were used to simulate the interactions between blocks and the Mohr-Coulomb law was used to regulate the contact behavior [10]. Two failure modes of mortar were investigated: tensile failure and shear failure. Tension failure is modeled in the DDA method as having no tension between blocks, while shear failure is modeled in DDA as having friction behavior between blocks. The stiffness of the springs in between

blocks was modeled to be proportional to the strength of mortar. This concept of artificial joints was adopted to refine the DDA method so that it can be used to analyze the continuous and discontinuous behavior of the masonry structure [10]. As for the reinforced concrete frame, it was modeled as triangular concrete subblocks, and the reinforcement and concrete were assumed to be in perfect bond. By validating the DDA numerical solutions with experimental results, the study concluded—using stress distributions of the framed masonry wall—that the behavior of masonry structures was highly influenced by the failure of the mortar joints. The study also showed that the triangular subblocks are capable of simulating the bending behavior of flexural elements. Furthermore, it was concluded that the completely infilled masonry wall largely increases the stiffness of the structure compared to the other two models, in addition to significantly affecting its behavior [10]. The study however overlooked investigating and considering factors such as the out-of-plane failure of the wall and the constitutive relations of brick, mortar and concrete.

Zarnic et al. [11] tested using a shake table two 1:4 scaled models of masonry infilled reinforced concrete frame buildings designed according to the Eurocode. The models were shaken with a series of horizontal sine dwell motions with gradually increasing amplitudes. During each test run, the specimens were tested with different simulated earthquakes, but with the similar resonant effect. The walls were primarily constructed using strong bricks and weak mortar. Due to this construction, cracks developed and propagated along the mortar beds without cracking of bricks. Damaged infills and overstrengthed frames apparently increased the base shear forces obtained from experiments. The study concluded that buildings with masonry infill walls designed according to Eurocodes are able to sustain relatively high dynamic excitations due to a high level of structural overstrength. In addition, the study showed that testing of infilled frame building models constructed in reduced scale following the true replica modelling rules can provide valuable information on the overall response of the real structure and variation of their dynamic characteristics due to damage development. The obtained experimental results were all validated using a computational model, and the pushover analysis method [11].

Henderson et al. [12] conducted over 700 tests, large- and small-scale over a period of five years as part of a static and dynamic experimental research program. Experiments were conducted in the laboratory as well as on existing structures. The purpose of the study was to assess the strength and behavior of unreinforced masonry walls, understand how the infill walls interact with the surrounding frames, determine whether in-plane and out-of-plane behavior are coupled, and try to develop a predictive analytical method that is more representative of the actual situation than conventional code procedures. Preliminary tests were conducted to determine the structural properties of existing and new masonry blocks, in addition to observing the out-of-plane behavior of an existing infill. The preliminary tests showed that the structural properties of new blocks do not vary much from those of old blocks. It was also noticed that the out-of-plane strength of an infill wall was largely greater than that predicted by conventional code procedures. Drawing from these observations and to better understand the effects of in-plane and out-of-plane loads on infill walls, 25 moderate- and full-scale tests were conducted on infill walls. Tests showed that unreinforced masonry infills were more ductile and resisted lateral loads more effectively than predicted by common design codes. Furthermore, tests confirmed that the load carrying capacity of the infill was considerably above the load that caused initial cracking, which was a significant departure from classical code approaches that assumed first cracking to be the failure of an unreinforced masonry wall. The study also demonstrated that modeling the behavior of the infill as a compression strut was likely to be the best predictor of overall wall capacity since diagonal cracking and corner crushing were identified as the predominant in-plane failures and the shear capacity of the masonry does not govern the capacity of the infill itself [12].

Candeias et al. [13] reported on an experimental program aimed at the quantification of vulnerability curves of typical Portuguese four-story unreinforced masonry buildings that are built without sufficient earthquake resistance capacity. The seismic performance of these buildings is known to be deficient, and vulnerability curves can help in the process of large-scale rehabilitation to improve their seismic performance. The observed behavior of these buildings when subjected to earthquake loadings is characterized by generalized cracking of the exterior walls and out-of-plane collapse. Four 1:3 scale

unreinforced masonry buildings with masonry shear walls and wood-framed floors were tested on a shake table. The dynamic tests on the shake table were performed by imposing time series of artificial accelerations compatible with the design response spectrum defined by the codes for the zone where the buildings fall. The results replicated the typical real-life collapse modes of these buildings, which includes the generalized cracking of the exterior walls followed by out-of-plane collapse [13]. The study lacked any numerical validation of the results and did not discuss how the failure patterns would differ according to whether there exists a reinforcement scheme or not.

Hashemi and Mosalam [14] attempted to develop a new modelling technique and study the behavior of reinforced concrete buildings with unreinforced masonry infill walls using an analytical and an experimental approach. While all past studies that investigated the behavior of infilled frames for in-plane and out-of-plane loading have been focused on single-frame single-bay, this study was done on a full 5-story structure with several bays and frames. Their modelling effort was concentrated on enabling accurate representation of the in-plane behavior of unreinforced masonry infill walls and refining the modelling techniques of hysteretic strength and stiffness degradation in reinforced concrete elements and joints. The masonry infill walls considered were made of clay bricks and were constructed to full scale. The prototype structure, scaled to 75% of its original design size, was tested on the shake table with emphasis on the middle bays of its first story. Different ground motions were used in the experiment. These ground motions were scaled to generate different levels of intensity and were applied unidirectional in the direction parallel to the unreinforced masonry infill wall [14].

The test structure was assumed as a single degree of freedom (SDOF) system. The test structure in itself represents a computational modelling of the full 5-story structure on OpenSees software. The relationship between demand parameters of the test structure and those of the prototype structure was established using computational modeling. The authors found that the unreinforced masonry wall had a significant role in the strength and ductility of the test structure: the structure became stiffer, the natural period of vibration of the structure become shorter, and the dissipated energy and damping coefficients increased. Locally, the load path and the distribution of forces were

changed, increasing the demand on the adjacent reinforcement concrete elements. At small forces, below those needed to overcome the static friction between the cracked surfaces, cracked walls acted as a whole, thus increasing the apparent stiffness of the system. The study observed that unreinforced masonry infill walls increased the shear demand on the diaphragm, and that as they started cracking, their effect on the structure diminished with the reinforced concrete frame taking the significant portion of the earthquake-induced forces. The study also showed that the cracking of the infills was characterized by 45 degrees shear cracks from the top corner of the wall to the bottom opposite corner. To validate the model, computational and experimental tests were conducted. For the computational tests, an equivalent strut was used to model the unreinforced masonry infill wall and the results were in good agreement with the experimental ones. However, when considering the computational model, the results were sometimes overestimating or underestimating several key parameters, meaning they were not representative of the actual experimental observations [14].

Meisl et al. [15] investigated the sensitivity of the rocking response of unreinforced masonry walls to the type of ground motion and the quality of the wall construction. Of the typical unreinforced masonry building damages, this study focused on out-of-plane failures of multi-wythe walls since they can result in collapse of the loadbearing walls and possibility of the subsequent total building collapse. This type of failure often happens due to inadequate anchorage of the walls to the floor diaphragms; this causes the wall to behave as a cantilever and topple when lateral loads push it beyond the point of static instability or half wall width. When the infill wall is sufficiently anchored to the floor diaphragms from the top and the bottom, its behavior is similar to vertical beams when in bending with end supports. In this study, walls were assumed to be sufficiently anchored to the floor diaphragms to produce the beam bending mode of out-of-plane failure, in which bending is in the direction of the wall height. Excessive bending causes large displacements at mid-height of the wall, rendering it unstable and vulnerable to collapse.

Shake table tests were conducted on four full-scale multi-wythe walls with varying construction quality and subjected to three different ground motions. Clay masonry

bricks and type O mortar were used. Recorded results showed that the displacement of the wall relative to its base is the key parameter in measuring wall stability. It was observed that under static conditions, when the relative displacement at the crack is equal to the wall width, the wall becomes unstable. In addition, once the wall cracks, it moves as two superimposed rigid rocking blocks. It was also noted that once the walls crack, they undergo a nonlinear force-displacement response. The study concluded that inadequate anchorage of walls to floor diaphragms is the most frequent cause of failure of unreinforced masonry infill walls. With sufficient anchorage to diaphragms, out-of-plane loaded unreinforced masonry walls were shown to crack above midheight and then rock as two rigid bodies without collapse. In this way, the wall maintains its stability until reaching a displacement at midheight equal to the wall's thickness. It was also concluded that walls built with a height to thickness ratio limit of nine, set by ASCE/SEI 41, have very low probability of failure [15].

Toranzo et al. [16] investigated a shake table test on a 2:5 frame wall system. This system is thought to help confined masonry rocking walls to resist seismic hazard. To reduce residual drifts and structural damage, confined-masonry rocking walls were adopted in the test. Previous studies showed that this type of walls had many advantages such as the ability to sustain large lateral displacements without much damage and having a re-centering mechanism that eliminates any residual deformations. Disadvantages of this type of walls include: unpredictable seismic response, low energy dissipation capacity, and potential large impact actions. To help eliminate these disadvantages, the study investigates the effectiveness of using an external linearly tapered steel cantilever Energy Dissipation Devices (EDD) system. The study suggested that, with careful design and placement, these devices can provide initial high-stiffness, provide a stable hysteretic response, avoid fracture before attaining high displacements, and ensure self-centering response of the walls. An additional feature of these devices is that they can transfer the wall shear force directly into the foundation, reducing the reliance on friction for shear transfer [16].

A test structure was used that represented a segment of a typical three-story building comprised of confined-masonry walls. Four aspects were addressed in the design

methodology: prevention of any residual displacements, control of the lateral drift of the structure, enforcement of the rocking mechanism of walls, and prevention of the structural damage under an earthquake defined by a 475 years return period. A shake table test was conducted on a 2:5 scale model frame-wall system. Large stresses were developed in the toes of the walls at the contact points between the foundation and the rocking wall. To avoid damage, a steel plate was used in the impacted region. Sixty (60) dynamic tests were run; some were used to observe the fidelity of the signal and others to observe the seismic performance of the structure. Experimental results showed excellent performance of the tested system, where limited damage was observed, no residual displacements were found, the lateral design capacity was retained, and the slabs preserved their vertical load capacity. By comparing several dynamic runs with and without the EDD systems, the strong dampening effects of the system used and its relatively high resistance to drift were noted. The only damage observed in the test structure was in some of the slabs that had a shallow groove. It was concluded that using confined masonry rocking walls minimizes the structural damage and residual drifts. It was also found that since rocking systems suffer from low inherent damping properties, the use of steel dissipating dampers at the base of the wall alleviated the problem. The paper demonstrated a major advantage of rocking systems which is self-centering; after the shaking has been concluded, no residual deformations were observed [16].

Bothara et al. [17] investigated the seismic performance of a 1:2 scale two story brick masonry building tested under earthquake ground motions on a shake table in two directions: longitudinal and transverse. The building represented a scaled model of an existing unreinforced masonry building in Christchurch, New Zealand that had a gable roof. A mortar mix of 1:1:6 (cement, lime, sand) was used to glue the bricks together and recommended practices such as soaking of bricks in water and dry mixing of mortar before adding water were adopted in the wall construction. The testing program aimed at investigating the seismic behavior of unreinforced masonry buildings and identifying their dynamic characteristics. The building was constructed using single wythe clay brick masonry laid in cement sand mortar. During each excitation, the cracks were accurately mapped and plotted and during the longitudinal shaking tests, no instability of any part of the model was observed. Cracking and rocking of the walls were observed.

Unlike the extent of damage seen in unreinforced masonry walls during moderate earthquakes, the tested model did not lose integrity or stability, nor did it show any sign of collapse even during high peak ground accelerations of 0.8g. These observations were justified by the study using the high quality control, the solid reinforced concrete foundation, the bond between orthogonal walls, the low span to depth ratio of walls, the reduction in out-of-plane moment of inertia and the fixity of loads on the diaphragms [17].

The study concluded that the damage increased with the increase in severity of the excitations applied to the building, but with no collapse occurring. Damage included global rocking of the piers and out-of-plane failure of the walls. This study validated previous theories which argued that gable walls are the most vulnerable part of an unreinforced masonry building. The study also noted that the concentration of high stresses leads to in-plane damage, while high response acceleration leads to out-of-plane damage. It was also shown that maintaining a good bond between orthogonal walls significantly strengthens the walls with respect to out-of-plane failure.

While much of the research has focused on modeling the behavior of masonry infills using various numerical and analytical approaches, little information exists on the strength of such walls under out-of-plane lateral loading. Design codes still consider cracking as the structural failure of these walls and encourage structural designers to consider infills as dead load only with no contribution to the strength of the structure. This research examines the strength and overall behavior of unreinforced masonry infill walls subjected to out-of-plane earthquake loads. It also investigates the adequacy of proposed approaches in modeling the strength and behavior of infill walls.

Chapter Three
Methodology

Research Aim and Objectives

The overall aim of this research is to investigate the dynamic response of moment resisting reinforced concrete frames with unreinforced masonry infill walls commonly used in residential and commercial building construction in Lebanon. The objectives set forth to achieve this aim are therefore established as follows:

1- Survey existing literature on the seismic behavior and testing of concrete masonry infills;
2- Survey the construction methods and materials used for this type of structures in the Near East Region;
3- Devise an experimental testing approach to conduct full dynamic load tests of scaled infill wall models using the same material and construction methods surveyed;
4- Run full dynamic load tests using out-of-plane displacements generated from a scaled real-life earthquake, and measure the dynamic response of the model using proper experimental instrumentation;
5- Analyze the results of the experimental tests to determine the overall behavior, as well as the stresses and displacements, incurred by infill walls under out-of-plane dynamic loading;
6- Compare the experimental results to commonly accepted analytical models; and
7- Formulate the findings into recommendations as to the appropriateness of the use of such structural elements in residential and commercial building construction.

Research Significance

Unreinforced concrete masonry infill wall construction in the Near East region suffers from lack of proper design codes, lack of uniform construction methods, and lack of material and construction quality control. The above, coupled with the absence of any

research on the behavior of such walls when exposed to out-of-plane seismic loads, makes them highly vulnerable to failure during earthquakes. The significance of this research lies in being the first to study the dynamic response of unreinforced concrete masonry infill walls as constructed in the Near East region. The results of this research can help to better understand the behavior of such walls under out-of-plane dynamic loads, and to formulate construction practices improvements and design recommendations to be used by engineers when designing such structural elements.

Current Methods and Materials

Figures 1 and 2 show the construction approach typically adopted for unreinforced concrete masonry infill walls in the region discussed. They showcase the poor quality adopted and bad construction techniques. By carefully examining the pictures, one can quickly notice the irregularities in the consecutive masonry courses, in particular the top most course. Unlike U.S. construction practices where the masonry walls are constructed before the casting of the roof slab and tie beams, infill walls are erected after the roof or subsequent floor slab is casted. This practice coupled with non-modular floor clearances, results in the majority of these infill walls having a top course with a height less than that of a full concrete masonry block. Masons faced with such situations tend to manually break the blocks using a hammer or use previously broken pieces of concrete masonry units and stuff them in the remaining gap to try and fill the void. These masonry pieces are glued together using mortar, creating a scenario in which the infill wall has no mechanical anchoring system to the slabs, and a very weak bond develops between the masonry wall and the surrounding concrete frame. In addition, by carefully inspecting Figures 1 and 2, it is clear that the mortar joints in between adjacent masonry blocks are not uniform in thickness. Furthermore, modular full length blocks are not always used in consecutive masonry courses. Adding to what has been already mentioned, many times portions of the walls extend beyond the limits of the slabs as can be seen in Figure 1.

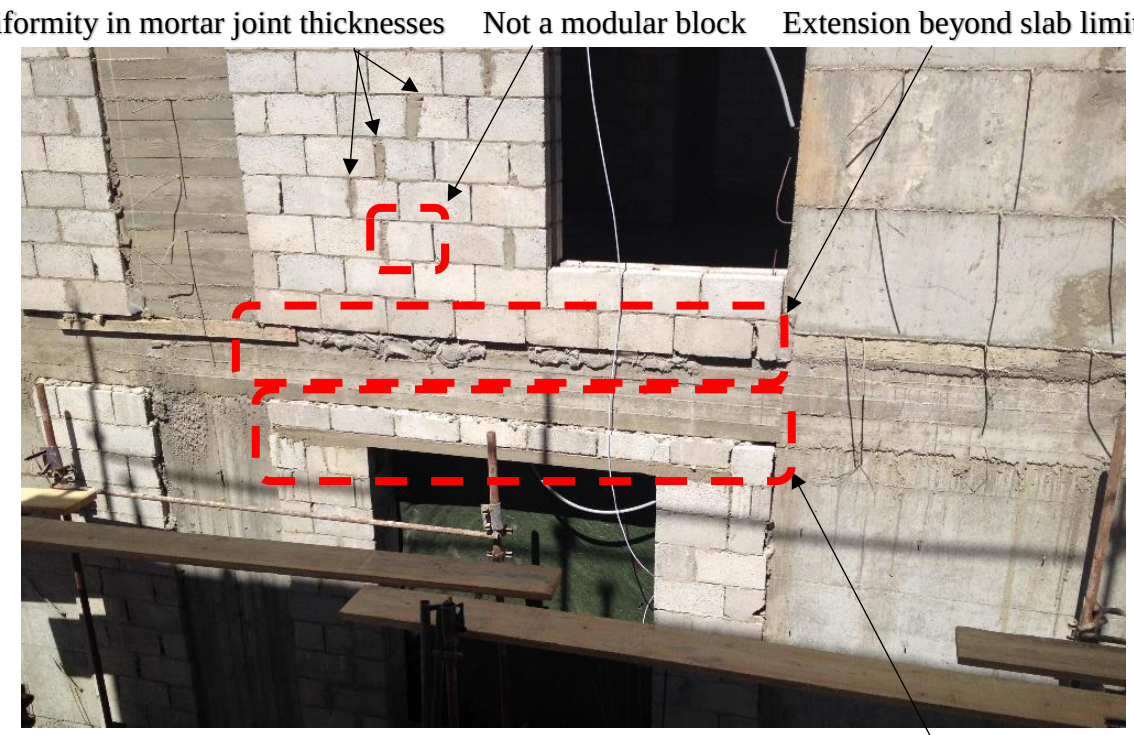

Figure 1: Example of the Construction Techniques

Figure 2: Another Example of the Construction Techniques

Figure 3 shows a typical 20 cm (8 inch) concrete masonry block used in the region for the construction of exterior infill walls. It can be seen that such blocks are not modular in that they do not have a two- or three-cell core that allows for half-size or third-size blocks to be manufactured or even saw-cut. It can also be seen that such blocks do not have open cells from both ends to allow for reinforcing, or even grouting.

Figure 3: Typical 20 cm (8 inches) Block: Bottom Side (Left) and Top Side (Right)

It is these inabilities to reinforce or grout the cells, use modular-cut blocks for corners or near openings, and properly anchor a full-sized top course to the roof slab, that make these masonry infill walls particularly vulnerable to out-of-plane moments resulting from seismic loads. This research will investigate the effects of these factors, and in particular the lack of sufficient anchorage of unreinforced masonry infill walls to nearby reinforced concrete frames, on their out-of-plane structural capacity.

Experimental Setup

Equipment Used

A three-dimensional Hexapod shake table manufactured by Quanser and comprised of six linear ball-screw actuators driven by six DC motors is used as an earthquake

simulator. This machine is capable of testing structures under six degrees of freedom, three of them being translational orthogonal (two horizontals and one vertical) and the other three being rotational (roll, pitch and yaw). The Hexapod unit is mounted with a 2.5 centimeters (1 inch) thick solid aluminum bearing plate that measures 100 x 100 centimeters (3.33 ft. x 3.33 ft.) in plan and has a weight of 65 kilograms (143 pounds). The plate is chosen with such a large thickness in order to have a much higher stiffness relative to that of tested masonry models. The maximum weight that the Hexapod is capable of moving is 250 kg (552 pounds), thus the net model weight the platform can carry is 165 kilograms (364 pounds). The ball screw actuators used by the machine are based on a high quality, low backlash linear guide with a total travel of 30 centimeters (11.8”) and are driven by high torque direct drive motors. A motor brake control uses the Hexapod’s brakes when the joints reach their limit. This ensures no damage is done to the device nor to the model load it carries. The maximum input acceleration and peak velocity for this shake table in all directions are 1g and 67 cm/s (26.4 inches/s), respectively. Maximum frequency for safe operation is 20 Hertz. The shake table is controlled through seamless integration of QUARC and MATLAB/Simulink [18] running on a parallel computer. Figure 4 shows an overview of the Quanser Hexapod shake table.

Figure 4: Hexapod Quanser Shake Table

Due to the model mass exceeding the upper limit of the shake table carrying capacity, a steel structure along with frictionless rollers mechanism was designed to carry the weight of the wall while the shake table provides only the lateral base displacement to the specimen. The structure consists of two steel rectangular plates, four steel angle plates, eight wheels and two thick elevated supports. The wheels are bolted to the bottom side of the rectangular plates, four to each plate and two to each end. To the top side of the plates, four L-shaped angles are bolted, two on each plate. The purpose of the angles is to prevent the concrete frame from overturning when displacing. This setup created a roller mechanism for displacing the wall while carrying the totality of the mass. The elevated supports ensured that the rollers and the bearing plate of the shake table were at the same level. This allowed the shake table to displace freely and provide only the base displacement input to the concrete frame. Figure 5 shows the details of the roller mechanism.

Figure 5: Adjusted Hexapod with Roller Supports

Laws of Similitude

Due to shake table size and weight limitations, much of the research done on the dynamic response of buildings to earthquake loads is performed using scaled models. One is however faced with a number of similitude difficulties when reduced scales are adopted in shake table testing. When constructing small scale specimens, a geometric

scale factor is applied and geometric similitude is reached. Since only the overall behavior of the structural system and its global failure mechanism are sought after in this research, a simple model similarity as opposed to a complete model similarity can be adopted.

To capture the behavior of structural elements and details, one would have to use full scale models. In the case of complete models, model materials are used to construct the structure. These materials have their stress-strain diagram scaled with the geometric scale of the whole structure in the direction of stresses. However, in the direction of the strains, the stress-strain diagram for model materials is the same as that for prototype materials. This also applies to the following properties: the specific weight, Poisson's ratio and the damping coefficients. On the other hand, for the case of simple models, prototype materials are adopted for the construction of the models [19].

The effects of many parameters including but not limited to stress and strain gradients and adhesion between masonry and mortar are altered when the physical dimensions of the model are reduced. In most cases, the possibility of modeling the influence of these parameters on the structural behavior to an acceptable degree of accuracy limits the reduction of the size of masonry building models. The smallest models suitable for maintaining the behavior of the structure were found to have a scale of 1:4 [20, 21]. If the seismic behavior of masonry buildings is studied by testing their models on earthquake simulators, the similitude between the phenomena observed on the buildings subjected to earthquakes and the models subjected to simulated ground motion should be considered as the most important measure of accuracy of testing procedures. In the same context, failure mechanisms and damage patterns obtained during the model tests should be similar to those observed on the prototype buildings after earthquakes. Similitude in dynamic behavior requires similar distribution of masses and stiffnesses along the height of the prototype and model. However, similitude in failure mechanisms requires similar working stress levels in the load-bearing and structural walls of the prototype and model masonry building.

For any structural system undergoing dynamic loading, the equation of motion can be written as shown in Equation 3-1 [22,23].

$$M_P\ddot{x}_P + C_P\dot{x}_P + R_P = -M_P\ddot{x}_{0_P} \quad (3\text{-}1)$$

where M_P = mass; $\ddot{x}_P$ = acceleration of the prototype; C_P = damping coefficient; $\dot{x}_P$ = velocity of the prototype; R_P = restoring force and $\ddot{x}_{0_P}$ = ground acceleration. The restoring force R_P could be written as shown in Equation 3-2:

$$R_P = K_P \times x_P \quad (3\text{-}2)$$

where K_P = stiffness of the prototype and x_P = displacement of the prototype.

Equation 3-1 could then be expressed as Equation 3-3:

$$M_P\ddot{x}_P + C_P\dot{x}_P + K_P x_P = -M_P\ddot{x}_{0_P} \quad (3\text{-}3)$$

If a general quantity Q_M has been measured on the model, Equation 3-4 can be used to calculate the prototype quantity Q_P [22,23,24].

$$Q_P = Q_M \times S_Q \quad (3\text{-}4)$$

where S_Q is the scale factor.

The relationships between the model and prototype quantities strongly depend on the materials used for the construction of the model. In the case of the usage of simple models, prototype materials are used for the construction of the models. The theoretically obtained scale factors which refer to the characteristic physical quantities and determine the dynamic behavior of structures are given in Table 1. Table 1 shows the resulting scale factors as well as well as the equations for the case of simple models [25].

Table 1: Scale Factors for the Case of Simple Model

Quantity	Equation	Simple Model
Length *(L)*	$S_L = L_P/L_M$	S_L
Volume *(V)*	$S_V = V_P/V_M$	S_L^3
Mass *(M)*	$S_M = M_P/M_M$	S_L^3
Moment of Inertia *(I)*	$S_I = I_P/I_M$	S_L^4
Strain *(ε)*	$S_\varepsilon = \varepsilon_P/\varepsilon_M$	1
Strength *(f')*	$S_{f'} = f'_P/f'_M$	1
Stress *(σ)*	$S_\sigma = \sigma_P/\sigma_M$	1
Modulus of Elasticity *(E)*	$S_E = E_P/E_M$	1
Specific Weight *(γ)*	$S_\gamma = \gamma_P/\gamma_M$	1
Stiffness *(K)*	$S_K = K_P/K_M$	S_L
Force *(F)*	$S_F = S_L^2 \times S_{f'}$	S_L^2
Time *(t)*	$S_t = S_L\sqrt{S_\gamma \times S_\varepsilon/S_{f'}}$	S_L
Frequency *(ω)*	$S_\omega = 1/S_L$	$1/S_L$
Displacement *(d)*	$S_d = S_L \times S_\varepsilon$	S_L
Velocity *(v)*	$S_v = S_\varepsilon\sqrt{S_{f'}/S_\gamma}$	1
Acceleration *(a)*	$S_a = S_{f'}/S_L S_\gamma$	$1/S_L$

The derivations of some of the scale factors found in Table 1 are presented in Equations 3-5 through Equation 3-12. The results of the derivations yield the scale factor to be used directly. For simplicity, when referring to a certain quantity in the equations, the scale factor for that quantity is automatically used.

$$M = \gamma \times V \Rightarrow S_M = S_\gamma \times S_V = 1 \times S_L^3 = S_L^3 \tag{3-5}$$

$$K = constant \times \frac{E \times I}{L^3} \Rightarrow S_K = constant \times \frac{1 \times S_L^4}{S_L^3} = S_L \tag{3-6}$$

$$F = K \times d \Rightarrow S_F = S_L \times S_L = S_L^2 \tag{3-7}$$

$$F = M \times a = M \times \frac{v}{T} = M \times \frac{d}{T^2} \tag{3-8}$$

$$\rightarrow T^2 = \frac{M \times d}{F} => S_{T^2} = \frac{S_L^3 \times S_L}{S_L^2} = S_L^2 \quad (3\text{-}9)$$

$$\rightarrow S_T = S_L \quad (3\text{-}10)$$

$$v = \frac{d}{T} => S_v = \frac{S_L}{S_L} = 1 \quad (3\text{-}11)$$

$$a = \frac{v}{T} => S_a = \frac{1}{S_L} \quad (3\text{-}12)$$

Model Scaling

The experimental program in this research is devised to reproduce a particular real scenario involving a real structure subjected to a real earthquake input motion. The prototype considered is a typical exterior reinforced concrete moment resisting frame with an unreinforced masonry infill wall located in the first story of a typical residential building. The prototype is a 3 meters high by 3 meters wide wall. The prototype is made of single wythe, 20 centimeters (8 inches) thick, commercial concrete masonry units as the one shown in Figure 3. The frame consists of two columns and two beams, both structural elements being 20 centimeters (8 inches) wide by 50 centimeters (20 inches) deep. Figure 6 shows the layout of the prototype. The prototype column reinforcement consists of 8 vertical bars of 14 millimeters (#4) diameter with 10 millimeters (#3) horizontal ties spaced at 20 centimeters (8 inches) on center. As for the prototype beams, the reinforcement consists of 4 longitudinal bars of 16 millimeters (#5) diameter bottom reinforcement and 2 longitudinal bars of 10 millimeters (#3) top reinforcement. Shear reinforcement consists of 10 millimeters (#3) stirrups spaced at 20 centimeters (8 inches) on center. The reinforcement provided for full scale concrete structures in Lebanon belong to grade 520 MPa (75 Ksi). Figure 7 shows the reinforcement for both columns and beams in the prototype.

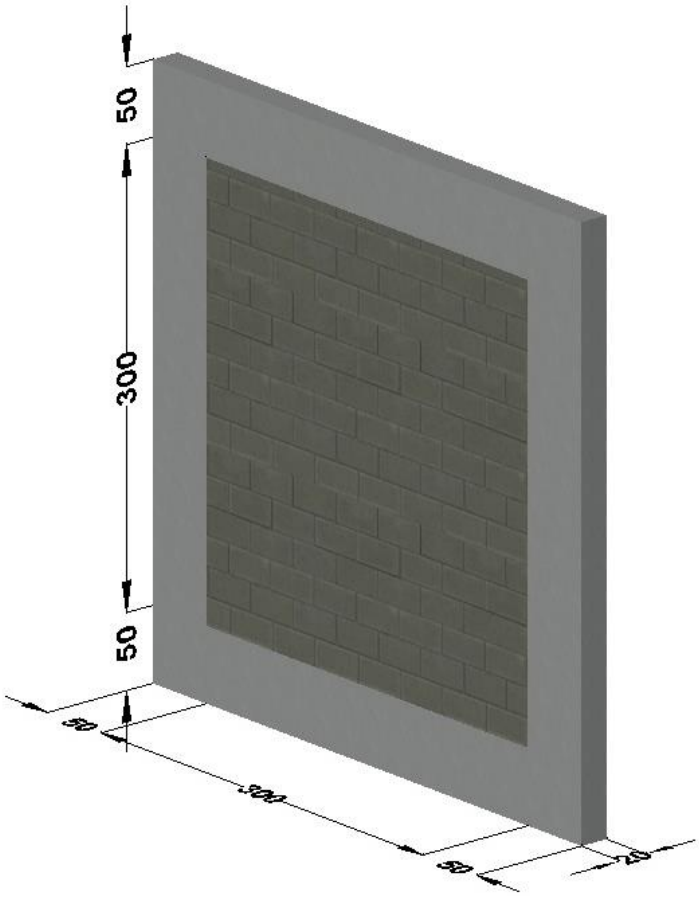

Figure 6: Prototype Wall Dimensions (in cm)

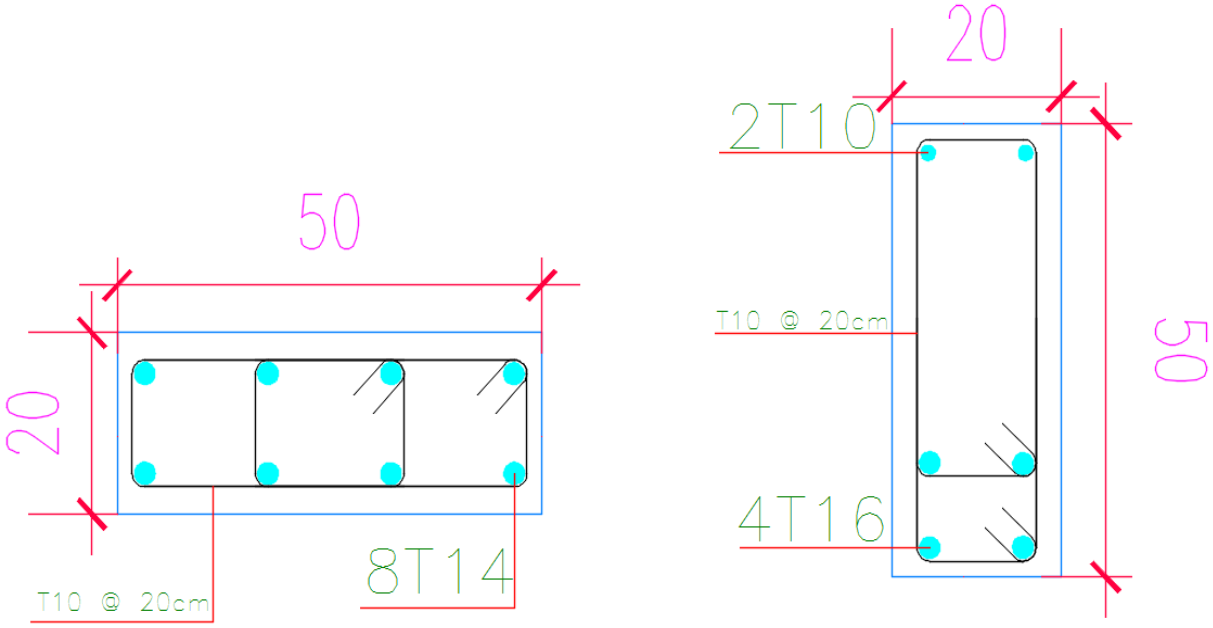

Figure 7: Prototype Column (Left) and Beam (Right) Structural Details (in cm)

In keeping with the weight limitations of the shake table, a scale of 3:10 is adopted for the simple model. This scale is well within the 1:4 scale limit suggested by existing literature [18,19] to be suitable for dynamic response testing. This scale results in a model 90 centimeters high by 90 centimeters wide. The beams and columns of the model will have a cross section of 6 centimeters (2.4 inches) wide by 15 centimeters (6 inches) deep. For the model frame having dimensions of 120 x 120 centimeters (4 ft. x 4 ft.), the bearing plate was aligned in order to fit the total length of the model on it as well as being perpendicular to one of the axes of movement of the hexapod. As for the steel reinforcement for the columns, the scaling results in 8 vertical bars of 6.5 millimeters (0.26 inches) diameter with 4.5 millimeters (0.18 inches) horizontal ties placed at 7 centimeters (2.75 inches) on center. The scaled steel reinforcement for the beams consists of 4 longitudinal bars of 6.5 millimeters (0.26 inches) diameter in the bottom and 2 longitudinal bars of 4.5 millimeters (0.18 inches) diameter top reinforcement. The shear reinforcement consists of 4.5 millimeters (0.18 inches) stirrups spaced at 7 centimeters (2.75 inches) on center. Figures 8 and 9 show the scaled model dimensions, and column and beam reinforcement, respectively.

Percentages of reinforcements for both prototype and model ranged between 1 and 1.3 percent. It should be noted that steel bars are supplied in nominal diameters. In addition, bars having a diameter less than 8 millimeters (0.32 inches) are provided in different grades than the ones with larger diameters. In order to meet the required percentages of steel reinforcement and to remain conservative, bars having a larger nominal diameter than the required ones were provided. This results in a scaling factor slightly different than the one provided in Table 1 for scaling of areas. However, since the objective of the research is to study the overall behavior of the masonry infill walls rather than the reinforced concrete frames, the small deviation from the scaling factor suggested in Table 1 can be conservatively ignored. Figures 10 and 11 show the actual reinforcement used in the construction of the frame, for a column and a beam.

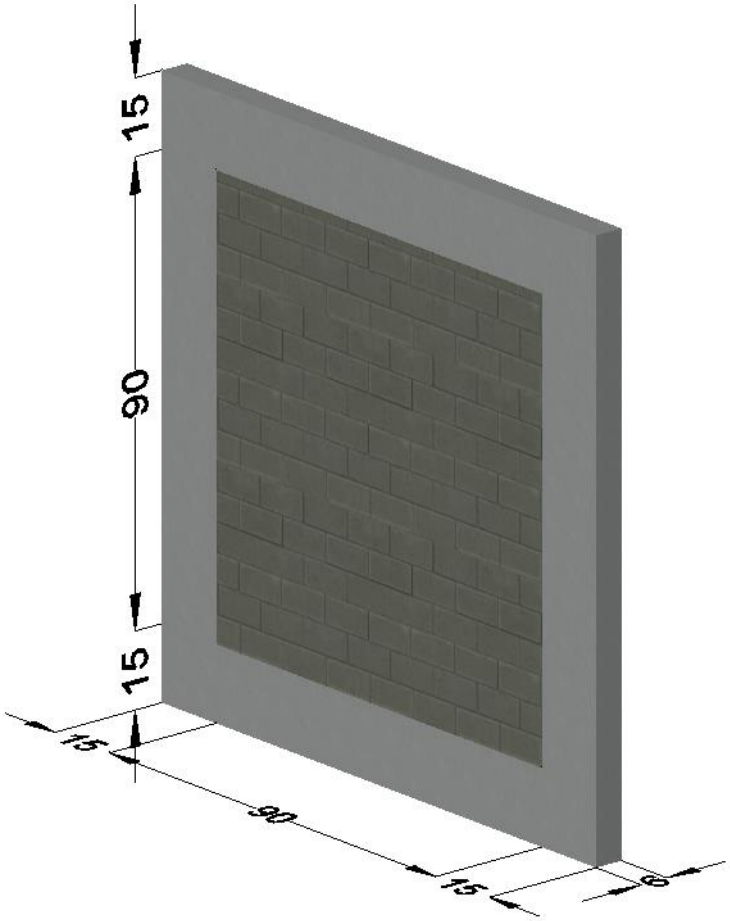

Figure 8: Model Wall Dimensions (in cm)

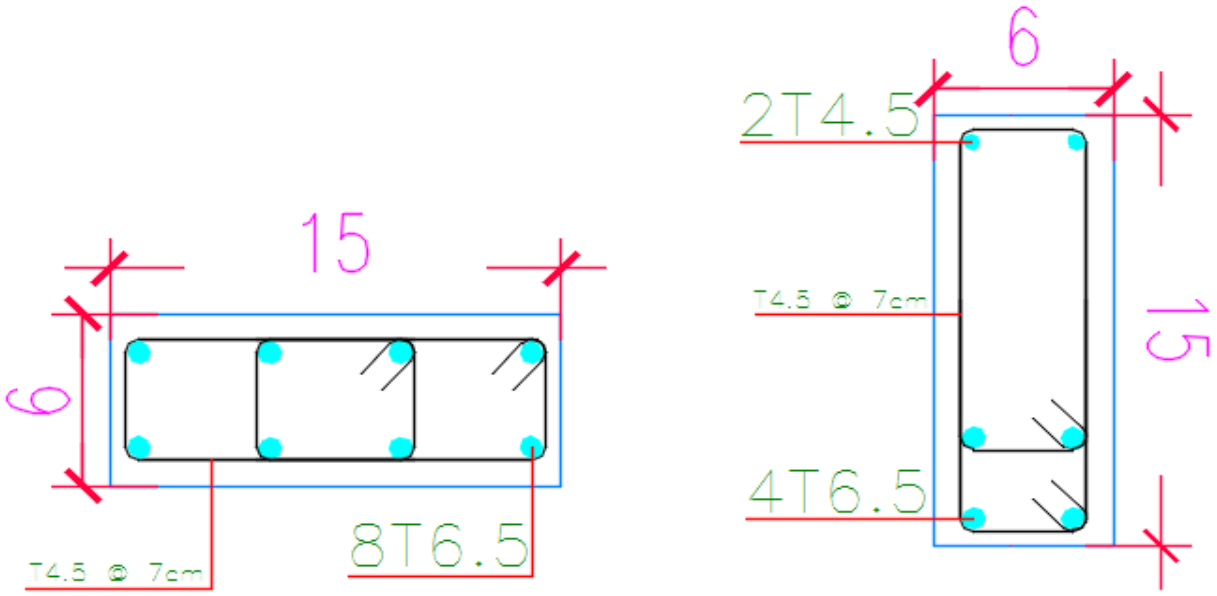

Figure 9: Model Column (Left) and Beam (Right) Structural Details (in cm)

Figure 10: Actual Beam Reinforcement

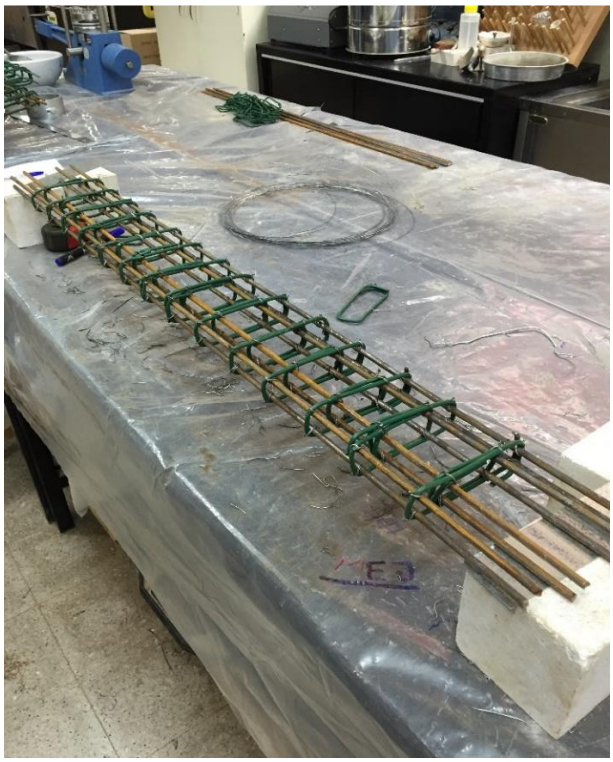

Figure 11: Actual Column Reinforcement

Model Masonry

The scale models of the infill walls are constructed in a running bond using the same methods used in the construction of the prototype and using concrete masonry units (CMUs) that are three tenth the size of a typical 20 centimeters (8 inches) block. Units are joined together using Type S masonry cement mortar for both bed and head joints, without the addition of any type of steel reinforcement. The model CMUs are fabricated in the same manner as the full-scale blocks using a scaled mold. Unit materials and mortar are essentially the same as those used in the full-scale construction except for the exclusion of large-sized aggregates from the mix design. The reduced-scale CMU blocks are 6 centimeters (2.36 inches) thick, 8 centimeters (3.15 inches) high and 15 centimeters (6 inches) long. The units have a net area of 55 cm^2 (8.5 in^2) and a net moment of inertia of 265 cm^4 (6.4 in^4). The full-scale blocks used in the prototype are 20 centimeters (8 inches) thick, 20 centimeters (8 inches) high and 40 centimeters (16 inches) long, with a net area of 400 cm^2 (62 in^2) and a net moment of inertia of 25,000 cm^4 (600 in^4). Figure 12 shows a comparison between the small-scale and full-scale blocks.

Figure 12: Prototype Block (Left) and Model Block (Right)

Material Testing

The masonry model units are supplied by a private manufacturer specialized in casting concrete masonry units. The blocks are constructed according to the provisions of ASTM C 129 – 11 [26] and are specified as nonloadbearing concrete masonry units. Three individual model blocks and three two-unit prisms were tested for compressive strength using a Tinius Olsen machine. The individual units had an average compressive strength of 11.52 MPa (1,700 psi), conforming to the ASTM C 129 – 11 [26] requirements. As for the masonry prisms, the mortar bed was expected to fail first before the crushing of the units. The mortar bed joints did indeed fail first and the average compression strength attained by the prisms was 14.17 MPa (2,050 psi). The type of failure observed was a Type 2—Cone and Shear failure—as described by ASTM C1314 – 11 [26]. Figure 13 shows the failure of one of the tested prisms.

Figure 13: Failure of One of the Prisms

The concrete used in the construction of the model is produced and mixed in the laboratory. The concrete mix used has the following proportions by volume: 1.2:1.8:3.2, (C:FA:CA). Type II cement is used and the water to cement ratio is 0.5. A Type F water

reducing and high range admixture is added to the mix, in compliance with ASTM C 494/ C 494M – 11 [26]. This mix resembles concrete mixes used on almost all residential building construction sites in the region, with an average compressive strength of 30 MPa (4,350 psi) to 35 MPa (5,100 psi). Five test cylinders are produced and moist-cured for uniaxial compression testing, the first cylinder is tested after 7 days of casting, two cylinders are tested after 14 days of casting, and the last two tested after 28 days of casting. Curing consisted of total submersion of the cylinders in water at 25^{o}C for the period between casting and testing. All the testing is performed using unbonded caps that consist of neoprene pads on the top surface of the cylinder to distribute the load evenly on the entire area. The type of failure observed in all the cylinders according to ASTM C 39/ C 39M – 11 [26], was Type 5—Side fractures on one end. This type of failure is a common occurrence when unbonded caps are used. Figure 14 shows the type of cylinder fractured exhibited during testing. Table 2 shows the results of the average compressive strengths of the cylinders. Figure 15 shows the compressive strength of the mix with respect to the age of concrete at the time of testing.

Figure 14: Type 5 - Side Fracture

Table 2: Average Compressive Strength of Concrete Cylinders

Cylinder Number	Concrete Age at Time of Test (days)	Average Concrete Compressive Strength
1	7	26.8 MPa (3,890 psi)
2	14	31.5 MPa (4,570 psi)
3	14	
4	28	35.3 MPa (5,120 psi)
5	28	

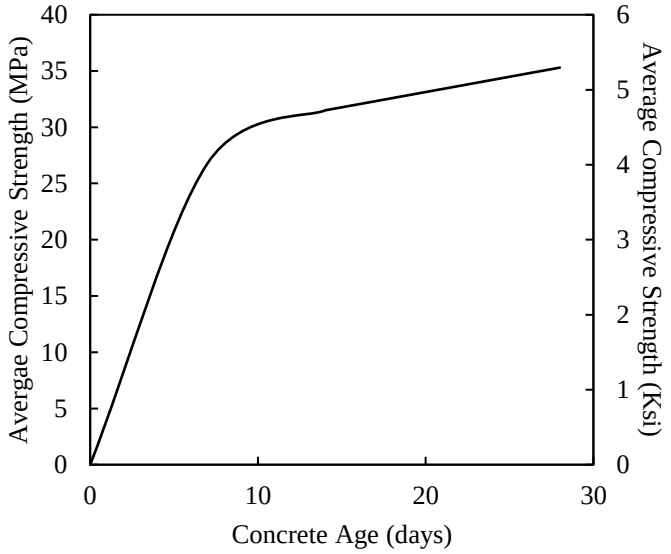

Figure 15: Compressive Strength of Concrete with Respect to Concrete Age

The steel bars used for the reinforcement of the concrete frames of the models are different from the ones commercially used in the construction and reinforcement of the prototype. The full scale bars are specified as Grade 75 (yield strength of 520 MPa or 75 Ksi), according to ASTM A 615/A 615M – 11 [26] whereas the reduced scale bars are specified as Grade 40 (yield strength of 280 MPa or 40 Ksi). A standard tension test was performed on six sample bars, three full scale and three reduced scale. Tables 3 and 4 show the minimum and maximum values for yielding, ultimate, and failure stresses and strains as well as ductility of the sample bars. The values obtained largely comply with the minimum values set in ASTM A 615/A 615M – 11 [26]. Figure 16 shows the average stress-strain diagram obtained for the tested full scale bars. Figure 17 shows the average stress-strain diagram obtained for the tested reduced scale bars. Figures 18 and

19 show the tensile testing done on the full scale rebars and the fracture of one of the samples used.

Table 3: Properties of Full Scale Steel Bars (Grade 75)

	Yield Strength	Ultimate Strength	Yield Strain	Ultimate Strain	Ductility ϕ
Min	578 MPa (83 Ksi)	674 MPa (97 Ksi)	3.3 %	11.2 %	1.17
Max	582 MPa (84 Ksi)	695 MPa (100 Ksi)	3.5 %	11.3 %	1.18
Mean	580 MPa (83 Ksi)	690 MPa (99 Ksi)	3.4 %	11.25 %	1.17

Table 4: Properties of Reduced Scale Steel Bars (Grade 40)

	Yield Strength	Ultimate Strength	Yield Strain	Ultimate Strain	Ductility ϕ
Min	268 MPa (39 Ksi)	378 MPa (55 Ksi)	0.96 %	20.1 %	1.41
Max	285 MPa (41 Ksi)	410 MPa (60 Ksi)	1.05 %	20.03 %	1.44
Mean	281 MPa (41 Ksi)	388 MPa (56 Ksi)	1 %	20.08 %	1.38

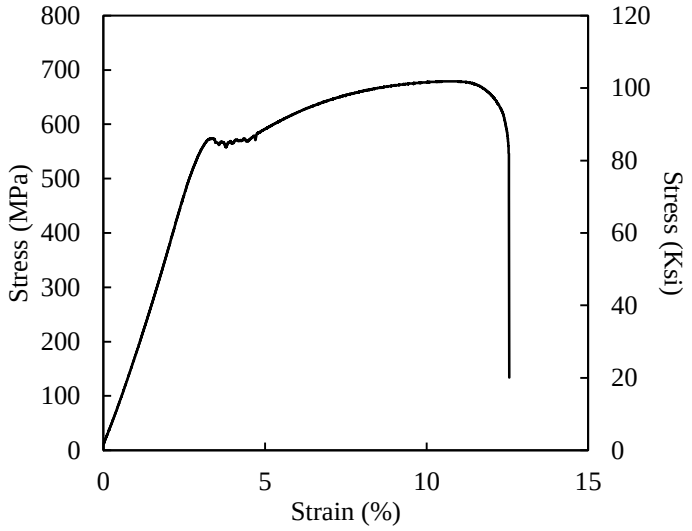

Figure 16: Average Stress-Strain Diagram for Full Scale Bars

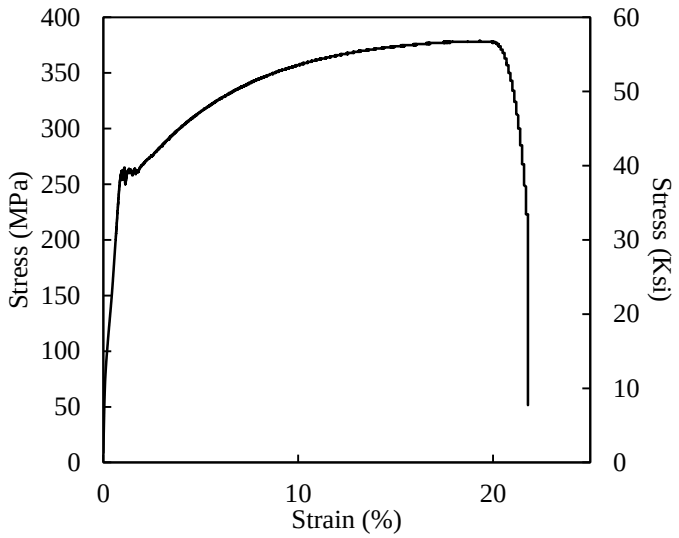

Figure 17: Average Stress-Strain Diagram for Reduced Scale Bars

Figure 18: Tensile Testing of Full Scale Rebar

Figure 19: Tensile Failure of Full Scale Rebar

The mortar mix used for the model walls has the same proportions by volume as the one commercially used on the prototype. The proportions consist of 1.2:2.5:0.6 (C:FA:WC) by volume. Six 5x5 centimeters (2 inches x 2 inches) mortar cubes were prepared and tested after 28 days of laboratory curing, according to ASTM C 109/C 109M – 11 [26]. Table 5 shows the average compressive strengths of the mortar cubes, and Figure 20 shows the failure of one of the mortar cubes tested.

Table 5: Average Compressive Strength of Mortar Cubes

Unit	Breaking Load (lbs.)	Average Breaking Load (lbs.)	Breaking Load (KN)	Average Breaking Load (KN)	Average Compressive Strength (psi)	Average Compressive Strength (MPa)
1	10,485	9,682	47	43	2,420.42	16.73
2	8,635		39			
3	8,850		39			
4	11,360		51			
5	9,620		43			
6	9,140		41			

Figure 20: Failure of One of the Mortar Cubes

Specimen Construction and Instrumentation

Three model frames with their respective masonry infill walls are constructed using the model material described. Figure 21 shows the frame's steel reinforcement, ties and formwork before casting of concrete.

Figure 21: Frame before Concrete Pouring

The first course of block is laid on the bottom beam, which is secured to the aluminum bearing plate using A325 (Group A) steel bolts imbedded in the concrete frame. The full reinforced concrete frame is cast in place before the masonry works begins, in keeping with currently adopted construction methods. Figure 22 shows the frame after casting of concrete.

Figure 22: Frame after Concrete Pouring

A half running bond is used to lay consecutive block courses. Whenever there is a need for a half block to complete one of the courses, scaled blocks are broken in half using small taps generated by handheld hammers, in much the same way as done in the construction of the prototype. The blocks are attached to their surrounding frame on all four sides using mortar only. Full mortar bedding is used for the construction of the model walls. Head and bed joints mortar thicknesses used in the construction of the prototypes are equal to 9.5 millimeters (3/8 inches). By applying the scaling factor of 3:10, head and bed joints mortar thicknesses used in the model wall are 3 millimeters (0.12 inches). To tie the wall from the top to the corresponding beam, broken pieces of scaled blocks are glued together using mortar and inserted on top of the final existing course in order to fill the remaining void. This is done because the remaining open space at the top of the wall represents an opening size that is less than that of the height of a full block.

After the completion of the construction, the external surface of the masonry is cleaned and parged with a very thin layer of cement paste. To make the crack markings more visible, a white paint is applied to the surface of the infill wall models. Figure 23 shows the concrete frame after the construction of the masonry infill wall. Figure 24 shows the masonry infill wall after plastering, and Figure 25 shows the same masonry infill wall after painting.

Figure 23: Concrete Frame after Construction of Masonry Infill Wall

Figure 24: Masonry Infill Wall after Plastering

Figure 25: Masonry Infill Wall after Painting

Two displacement transducers mounted on a nearby fixed structure measure the story displacements at the center of the two top beam-column joints. Two strain gauges on the bottom of the reinforcing steel bars of the columns provide strain readings for calculation of axial forces and moments in the frame members. Strain gauging of reinforcing bars is most useful in providing important information regarding the different performance levels of the models, such as point of first yield and attainment of failure strain level. Even though the objective of this research is the global behavior of the model, the strain gauges can provide critical data that can be crucial to the understanding of the model behavior. Eight additional strain gauges are used on the masonry wall, four on each side. The first set of two is placed at the joint between the bottom beam and the first course of masonry in the wall. The second, third and fourth sets of strain gauges are placed at one quarter, one half, and three quarters of the height of the wall, respectively. This instrumentation pattern is replicated on the other side of the specimen. For this configuration, twelve channels of data are monitored for each test run [27]. A schematic depicting the instrumentation used on the model is shown in Figure 26. The actual wall with all instrumentation before testing is shown in Figure 27.

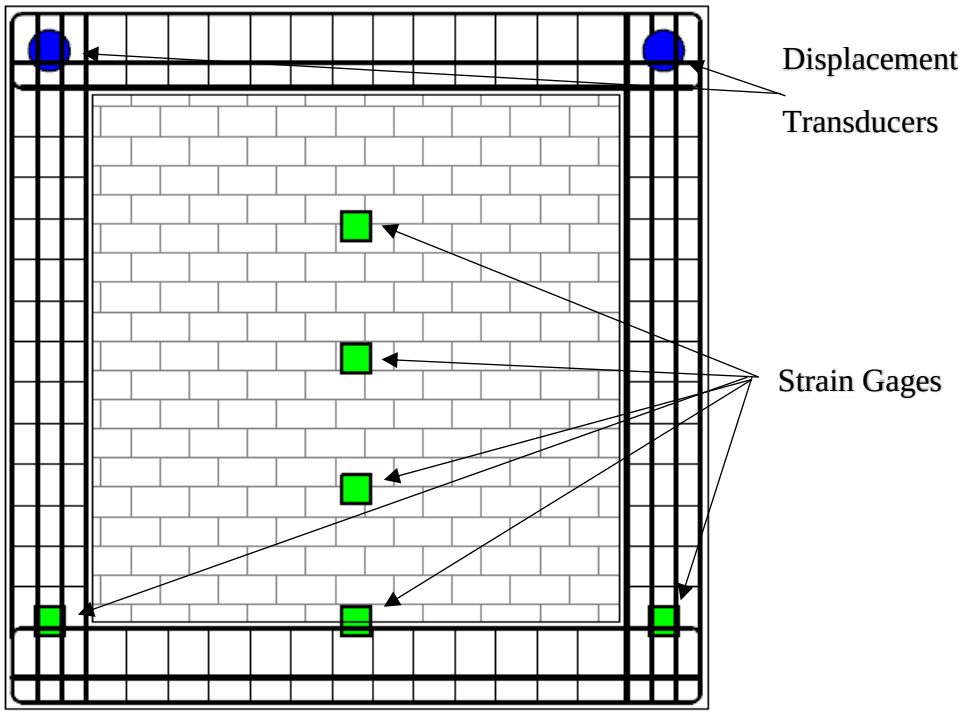

Figure 26: Schematic of Instrumentation

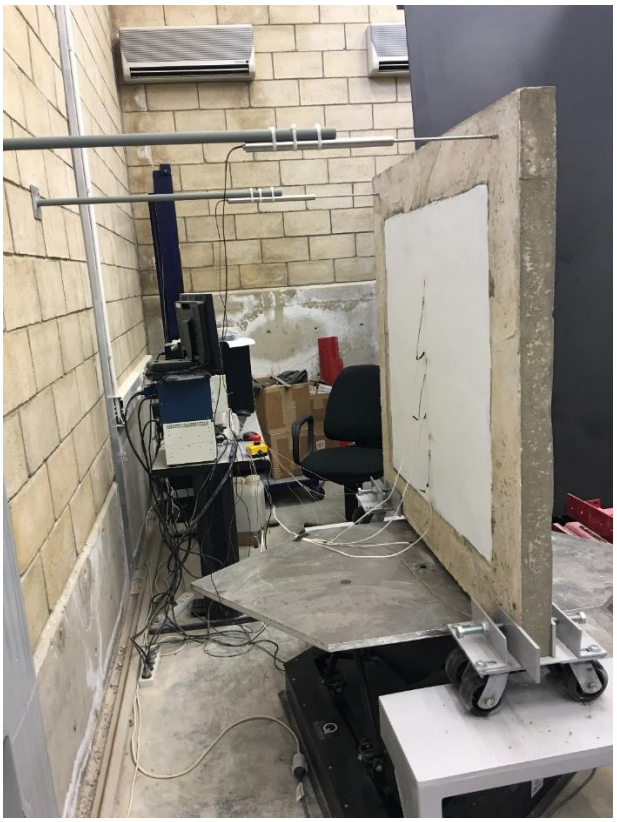

Figure 27: Frame with Instrumentation before Testing

Dynamic Loading

By testing small-scale masonry building models, only the behavior of the structural system and its failure mechanism can be determined. The detailed behavior of the structural elements cannot be determined since the reduction of the physical dimensions of the model lead to a change in the effects of many parameters on the overall behavior of these elements. These parameters include but are not limited to stress strain gradients, bond between mortar and surrounding frame, and adhesion between mortar and masonry units [28]. A real earthquake record is selected and used for this research. Base motions are patterned after the North South (NS) component motion measured at El Centro, California in 1940 in the Imperial Valley, which is a typical earthquake whose accelerations are well within what can be encountered in the Near East Region. The original El Centro 1940 North South component records are obtained from the United States Geological Survey (USGS) website [29]. The data includes the ground acceleration in terms of the gravitational acceleration and the time in seconds. Simpson's numerical method [30] is used to perform a double integration on the acceleration data points in order to obtain first, the ground velocity, and then the ground displacement. Equation 3-13 is applied on the acceleration data, where the smooth function *f(x)* defined over an interval [a, b] represents the acceleration values with respect to the time step chosen. Interval [a, b] represents the time domain boundaries of function *f(x)*, mainly time t_0 = 0 seconds and time t_{3000} = 60 seconds. Since the time step of 0.02 seconds (variable *h* in equation 3-13) is already provided in the original data extracted from the USGS archives, *n* takes the value of 3000, which is the number of data points used in the original data set.

$$\int_a^b f(x)dx \approx \frac{h}{3}\left[f(x_0) + 2\sum_{j=1}^{\frac{n}{2}-1} f\left(x_{2j}\right) + 4\sum_{j=1}^{\frac{n}{2}} f(x_{2j-1}) + f(x_n)\right] \qquad (3\text{-}13)$$

where $x_j = a + jh$ for $j = 0, 1, \ldots, n-1, n$ with $h = \frac{b-a}{n}$ and $x_0 = a$, $x_n = b$

For simplicity, Equation 3-13 can be written as Equation 3-14 as shown below:

$$\int_a^b f(x)dx \approx \frac{h}{3}[f(x_0) + 4f(x_1) + 2f(x_2) + 4f(x_3) + 2f(x_4) + \cdots + 4f(x_{n-1}) + f(x_n)] \quad (3\text{-}14)$$

The laws of similitude dictate that, for simple models, the time-scale factor should be equal to the length scale factor if velocities are to be consistent with the prototype. Since the shake table has a maximum frequency of 20 Hertz, yielding a time step of 0.05 seconds between data points, the original earthquake records have to be modified to meet these limitations. The original records have a time step increment of 0.02 seconds and therefore some of the data points are removed to increase the time step to 0.18 seconds. This, in-turn, modifies the frequency of the original records to 5.5 Hertz. By applying the scale factor of 3:10, the resulting time step has a value of 0.054 seconds and the frequency of vibrations obtained is about 18.5 Hertz—well within the capacity limitations of the shake table. It is worth noting that in order to remain on the conservative side when modifying the original earthquake records, the maximum displacement is always used when merging several data points into one. This ensures that, in order to fit the frequency limitation of the shake table used, the maximum values for acceleration, velocity, and displacement are maintained.

Figures 28, 29, and 30 show the acceleration, velocity and displacement profiles of the original earthquake record versus time, respectively. Figure 31 shows the displacement time history after being modified to meet the frequency limitations of the shake table. Figure 32 shows the scaled displacement time history used as base motion input to the shake table. The model wall is constructed in such a way that the dynamic forces generated by the shake table are being applied along a direction perpendicularly to the plane of the wall, thus inducing out-of-plane bending moments on the unreinforced masonry infill wall.

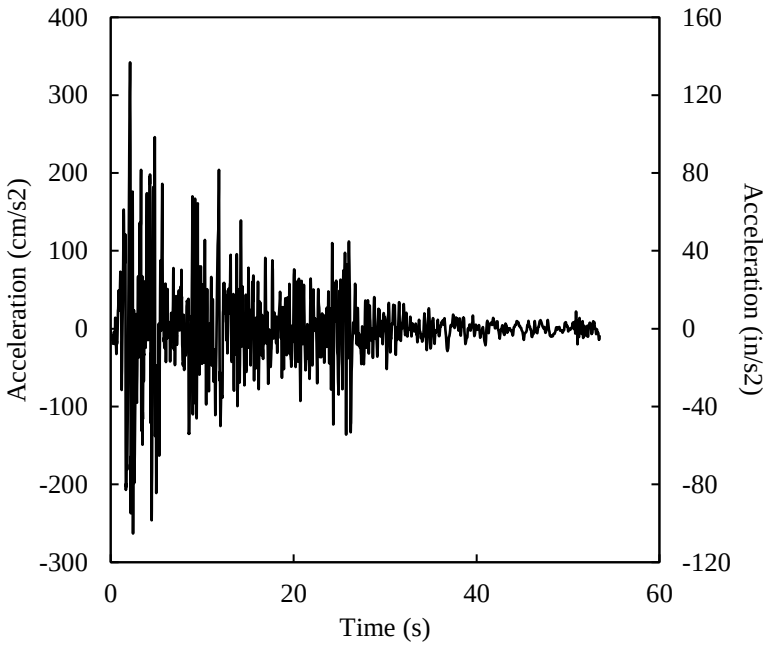

Figure 28: Acceleration Time History of Original Record

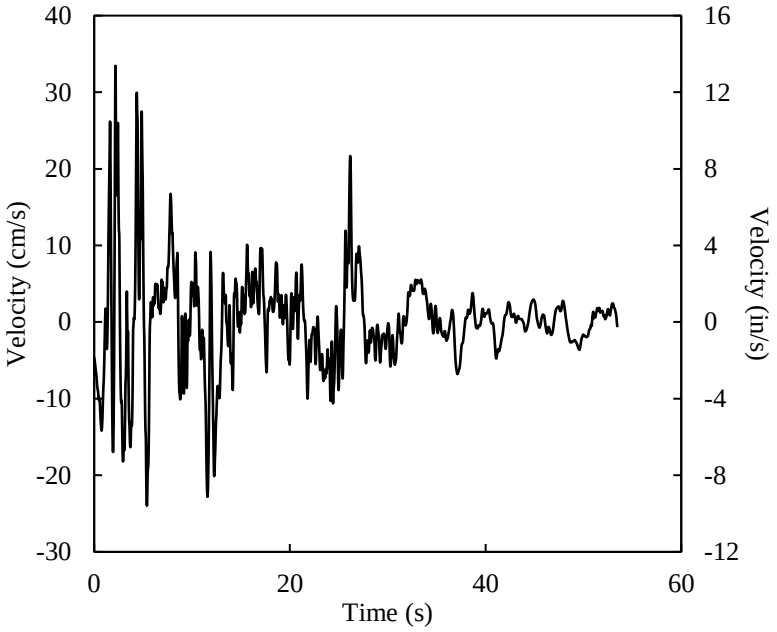

Figure 29: Velocity Time History of Original Record

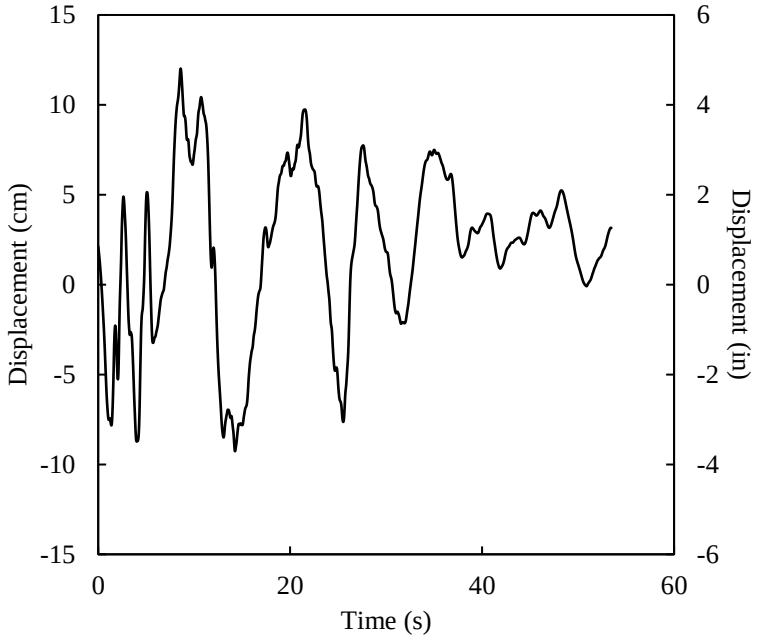

Figure 30: Displacement Time History of Original Record

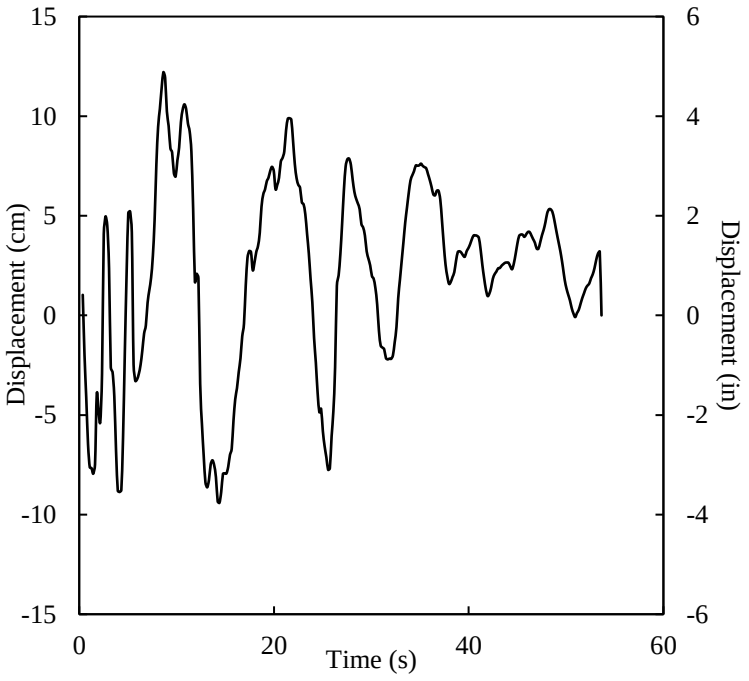

Figure 31: Displacement Time History Based on Modified Data

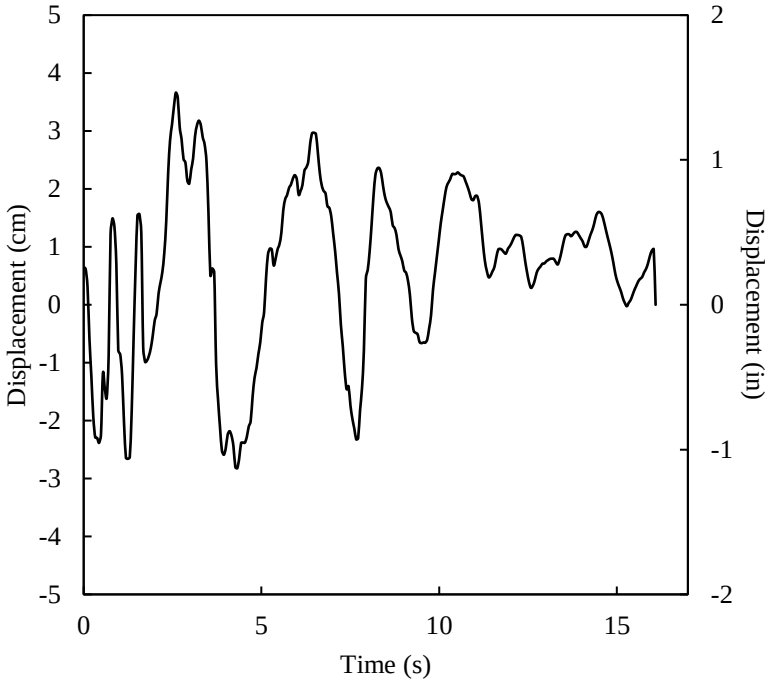

Figure 32: Scaled Displacement Time History

Chapter Four
Results and Analysis

The masonry infill walls specimens were subjected to out-of-plane scaled ground displacements of the 1940 El Centro earthquake. Each model specimen is subjected to four successive load tests. In order to study the strength and overall behavior up to failure of the infill walls, the input time history base displacement was multiplied by an amplification factor of 1, 1.5, 1.8 and 2. The maximum amplification factor was dictated by the displacement limitations of the shake table. The original scaled base displacement was factored by a gradually increasing term until failure occurred or the shake table reached its displacement capacity, whichever came first.

During each test run, the data from the data acquisition system (DAQ) is acquired and fed into LabVIEW® [31]. The frame is inspected for visible cracks after the load test is concluded. The experimental setup is recalibrated following each load test. Strains and displacements are measured for each specimen under each load test using the instrumentation described in Chapter 3. For each input data coupled with an amplification factor used, the values obtained from testing the three masonry walls are averaged. The strains obtained are compared to the theoretical tensile strain values required for the occurrence of micro cracking and visible cracking in mortar and concrete. The strains in the steel rebar are compared to the yield strains of the steel used. The stresses are obtained from the strains by applying a linear relationship between them using Young's modulus of elasticity E for each material. The micro cracking tensile strains for mortar and concrete are obtained by dividing the respective tensile strength by its respective modulus of elasticity. The visible cracking tensile strain for mortar and concrete are obtained from the factors developed by Hajali et al. [32].

The material properties used in the specimens are summarized below:

Concrete

$$f_c' = 35.3\ MPa\ (5120\ psi) \quad (4\text{-}1)$$

$$f_t = 4\ MPa\ (580\ psi) \quad (4\text{-}2)$$

$$E_c = 4700\sqrt{f_c'} = 28{,}000\ MPa\ (4{,}060{,}000\ psi) \quad (4\text{-}3)$$

$$\varepsilon_{Micro\ Cracking} = \frac{f_t}{E_c} = 1.43\ \times 10^{-4} \quad (4\text{-}4)$$

$$\varepsilon_{Visible\ Cracking} = \varepsilon_{Micro\ Cracking} \times 7.25 = 1.04 \times 10^{-3} \quad (4\text{-}5)$$

$$\sigma_{Micro\ Cracking} = f_t = 4\ MPa\ (580\ psi) \quad (4\text{-}6)$$

$$\sigma_{Visible\ Cracking} = \varepsilon_{Visible\ Cracking} \times E_c = 29.1\ MPa\ (4200\ psi) \quad (4\text{-}7)$$

Steel

$$f_y = 281\ MPa\ (41{,}000\ psi) \quad (4\text{-}8)$$

$$\epsilon_y = 0.01 \quad (4\text{-}9)$$

$$E_s = \frac{f_y}{\varepsilon_y} = 28{,}100\ MPa\ (41{,}000{,}000\ psi) \quad (4\text{-}10)$$

$$\sigma_y = f_y = 281\ MPa\ (41{,}000\ psi) \quad (4\text{-}11)$$

Mortar

$$f_m' = 14.2\ MPa\ (2{,}050\ psi) \quad (4\text{-}12)$$

$$f_t = 1.5\ MPa\ (220\ psi) \quad (4\text{-}13)$$

$$E_m = 15{,}057\ MPa\ (2{,}184{,}000\ psi) \quad (4\text{-}14)$$

$$\varepsilon_{Micro\ Cracking} = \frac{f_t}{E_m} = 9.96\ \times 10^{-5} \quad (4\text{-}15)$$

$$\varepsilon_{Visible\ Cracking} = \varepsilon_{Micro\ Cracking} \times 7.25 = 7.22 \times 10^{-4} \quad (4\text{-}16)$$

$$\sigma_{Micro\ Cracking} = f_t = 1.5\ MPa\ (220\ psi) \quad (4\text{-}17)$$

$$\sigma_{Visible\ Cracking} = \varepsilon_{Visible\ Cracking} \times E_m = 10.9\ MPa\ (1600\ psi) \quad (4\text{-}18)$$

Note that the color coding for the figures matches the curves of the different graphs. Only the back face of the masonry infill was considered since it represented the highest values. Additionally, positive strain values represent an opening in the joint, which is in tension, and negative strain values show a closure in the joint, typically a compression.

The following results represent only the data acquired from the maximum amplification factor of 2 used in the tests.

Results Acquired from Shake Table Testing

Figure 33 shows the placement of the four strain gages on the back face of the masonry infill wall. Figures 34 through 41 show the results recorded by the data acquisition system for the strains and stresses, respectively. The plots also show the material limits discussed previously.

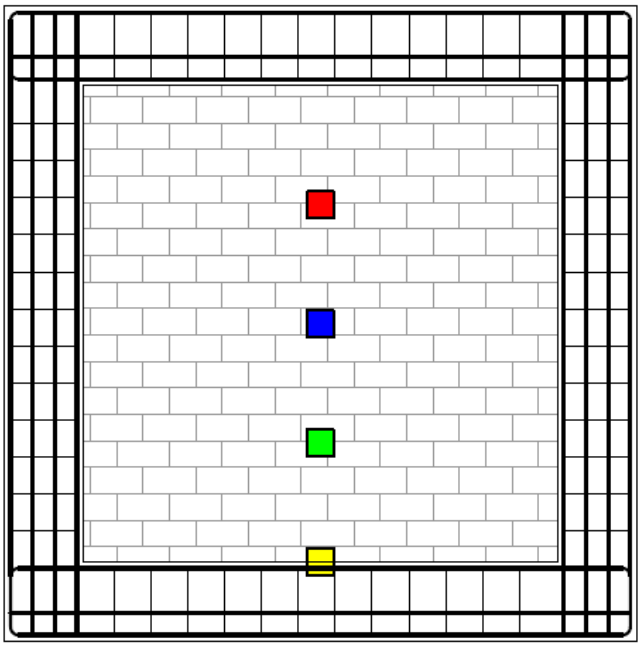

Figure 33: Location of Strain Gages on Back Face of the Specimens

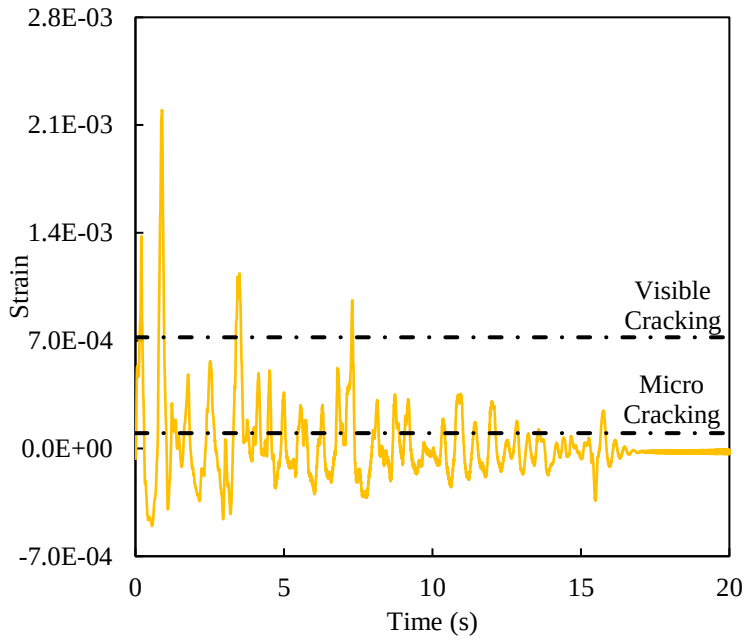

Figure 34: Strain Values Recorded at the Mortar Joint between the First Masonry Course and the Concrete Beam

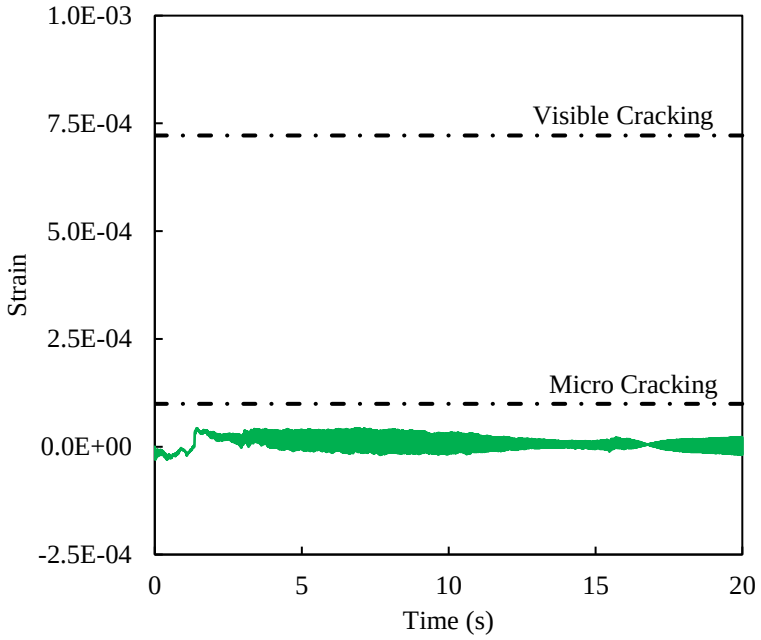

Figure 35: Strain Values Recorded at the Mortar Joint at Quarter Height

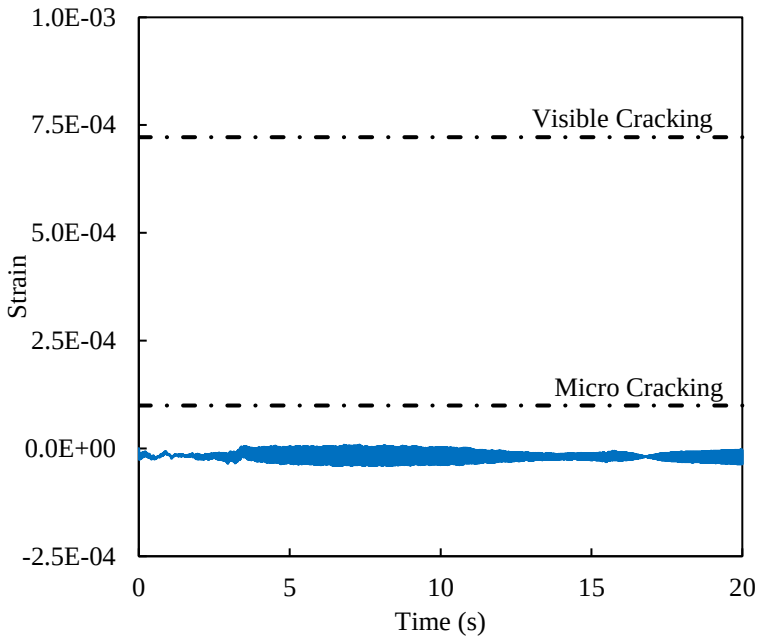

Figure 36: Strain Values Recorded at the Mortar Joint at Mid Height

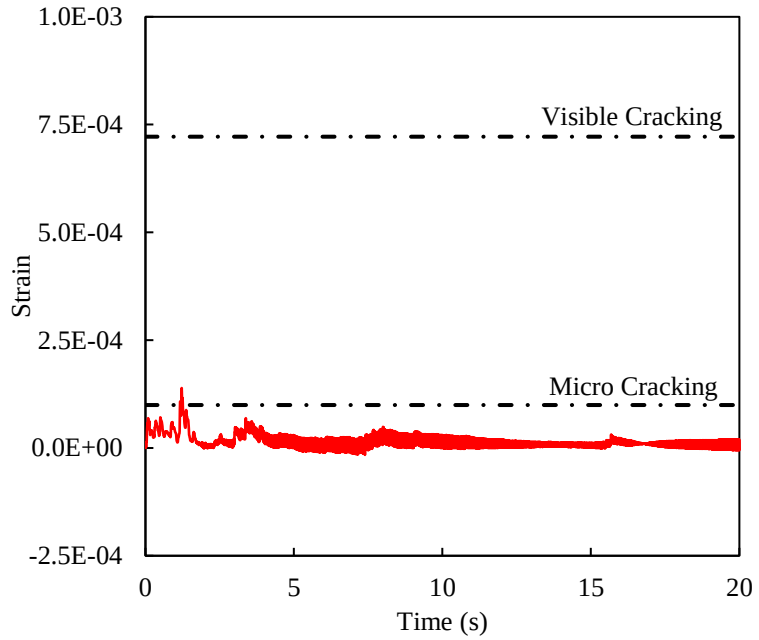

Figure 37: Strain Values Recorded at the Mortar Joint at Three Quarters Height

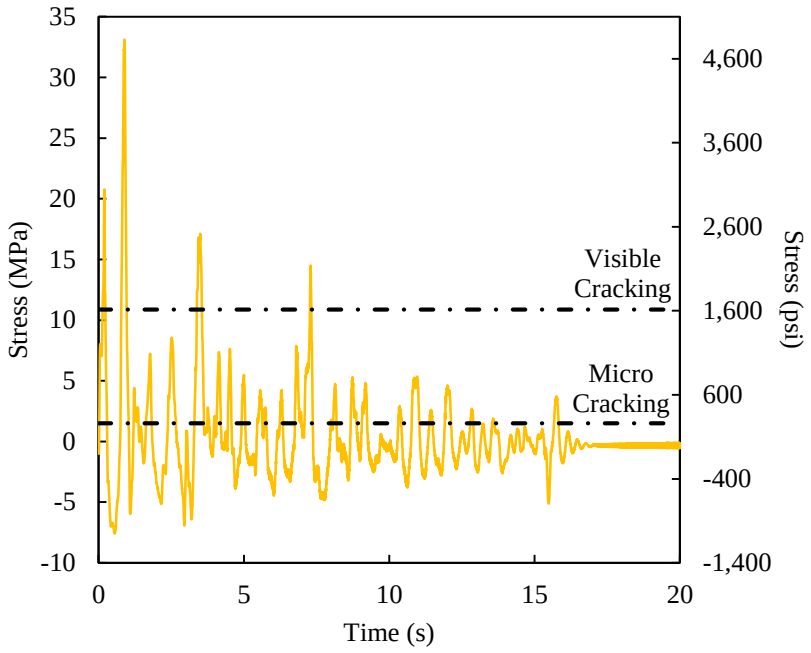

Figure 38: Stress Values Calculated at the Mortar Joint between the First Masonry Course and the Concrete Beam

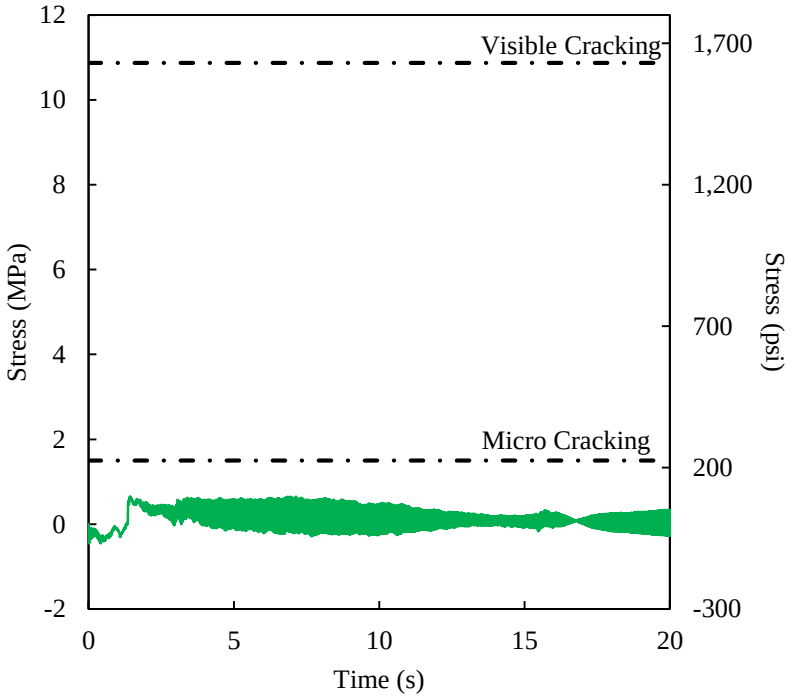

Figure 39: Stress Values Calculated at the Mortar Joint at Quarter Height

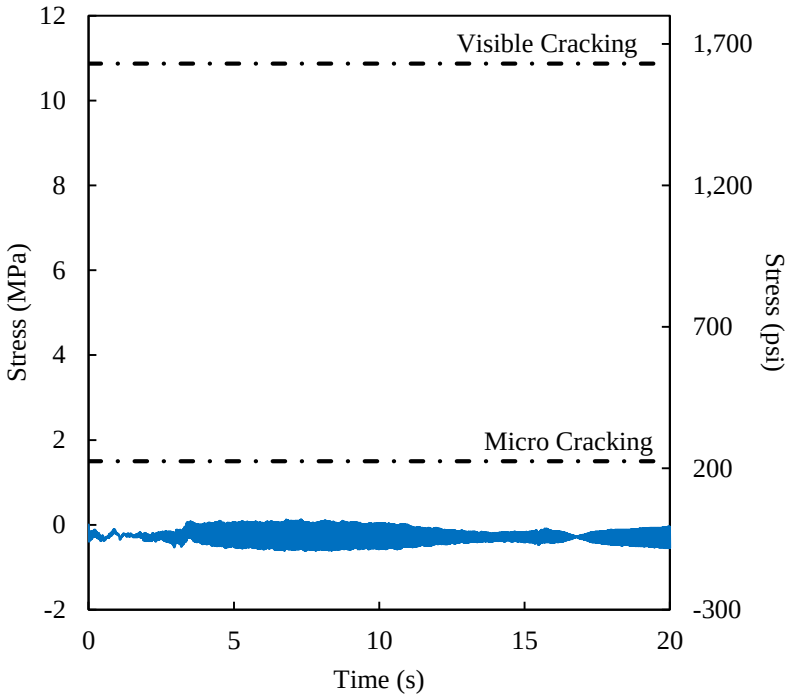

Figure 40: Stress Values Calculated at the Mortar Joint at Mid Height

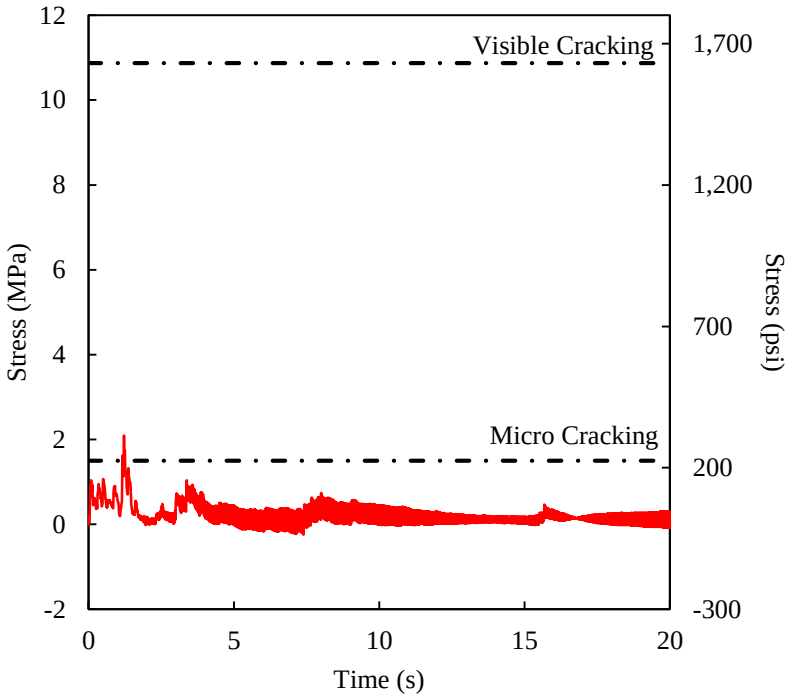

Figure 41: Stress Values Calculated at the Mortar Joint at Three Quarters Height

It can be clearly seen that the bottom strain gage, which captures the behavior of the mortar joint between the concrete frame and masonry infill, recorded the highest variations of strain. This is due to the opening and closing of the joint with the back and forth transverse movement and bending of the frame, which creates positive and negative strains. Even though the visible cracking limit for the displacement was surpassed in several short instances, no visible cracking could be observed on the wall itself. Figures 42 and 43 show the front face and back face of the wall after the testing occurred.

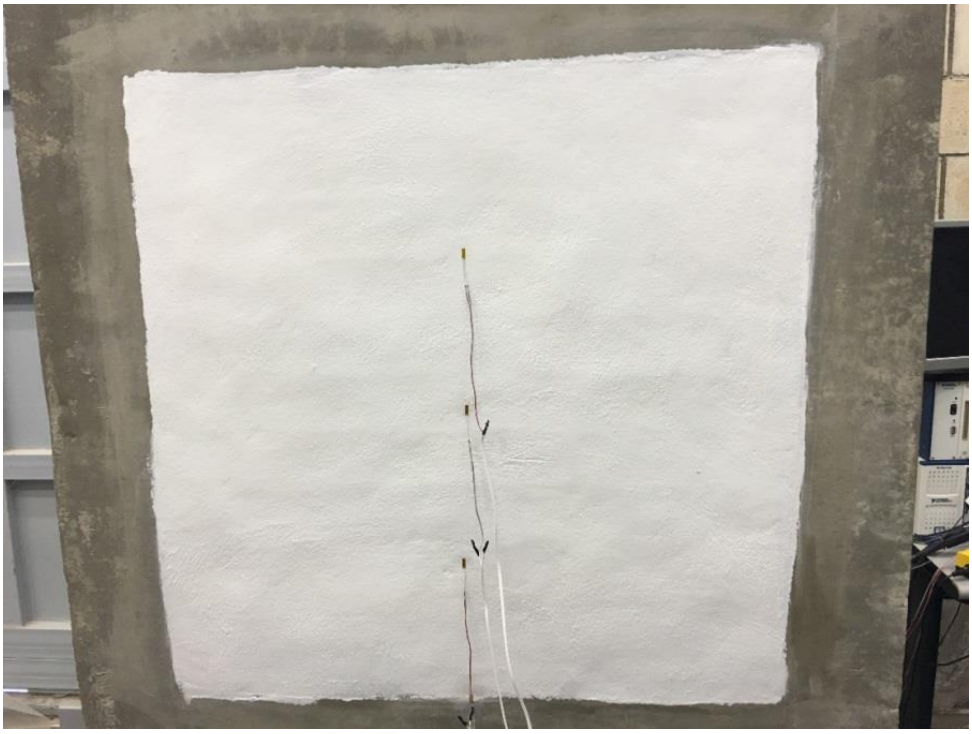

Figure 42: Front Face after Testing

Figure 43: Back Face after Testing

Figure 44 shows the placement of the strain gages on the steel rebar inside the concrete frame. Figures 45 through 48 show the strain and stress values recorded by the data acquisition system for the strains and stresses, respectively. The plots also show the micro cracking and visible cracking limitations for concrete. Figures 49 through 52 show the strain and stress values, respectively, recorded for the steel rebar along with the yield strength limitations of the material.

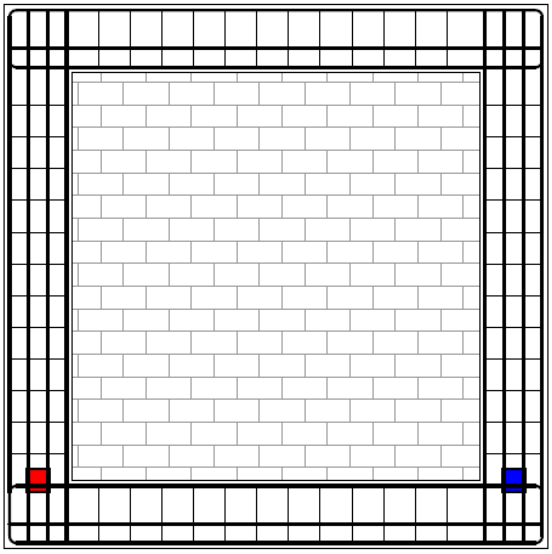

Figure 44: Strain Gages Location

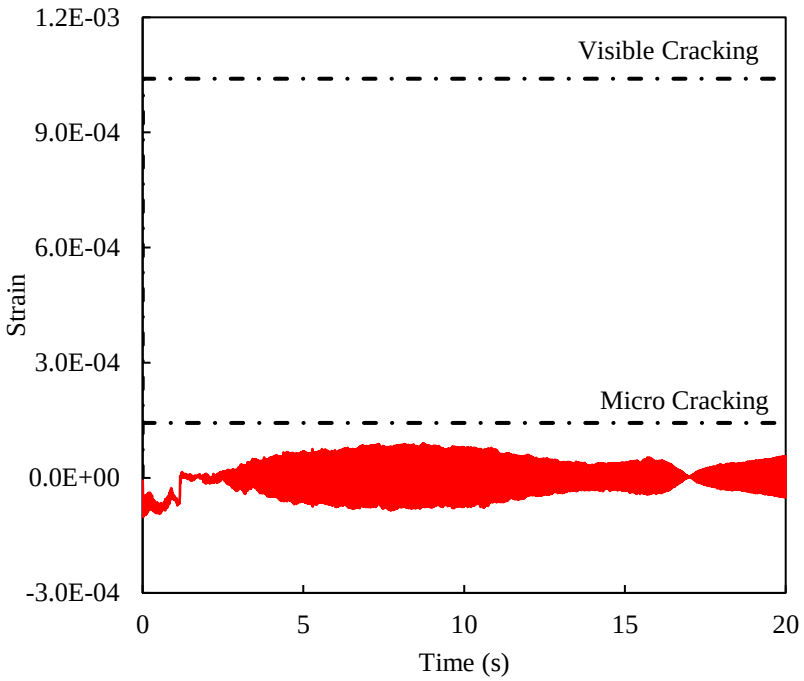

Figure 45: Strain Values for Concrete (Left Column)

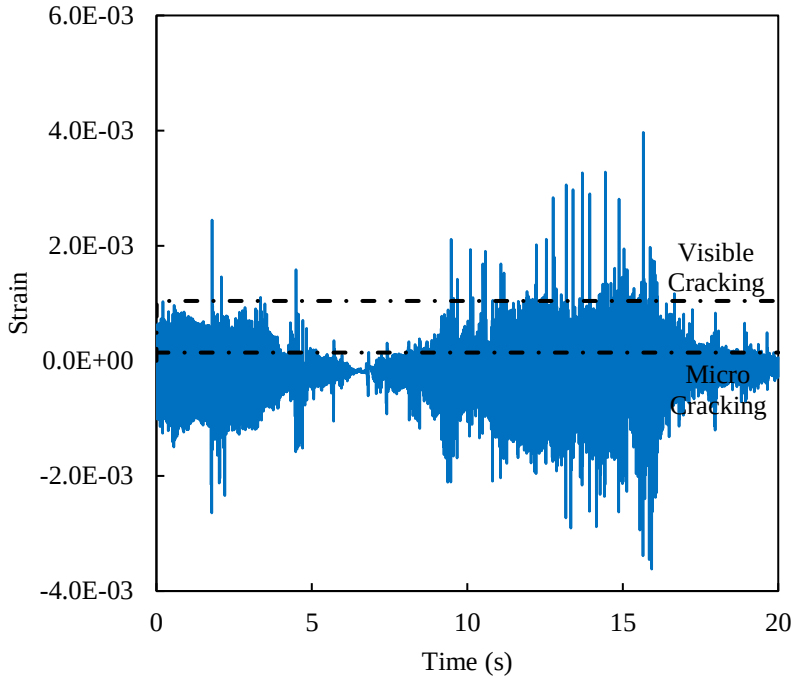

Figure 46: Strain Values for Concrete (Right Column)

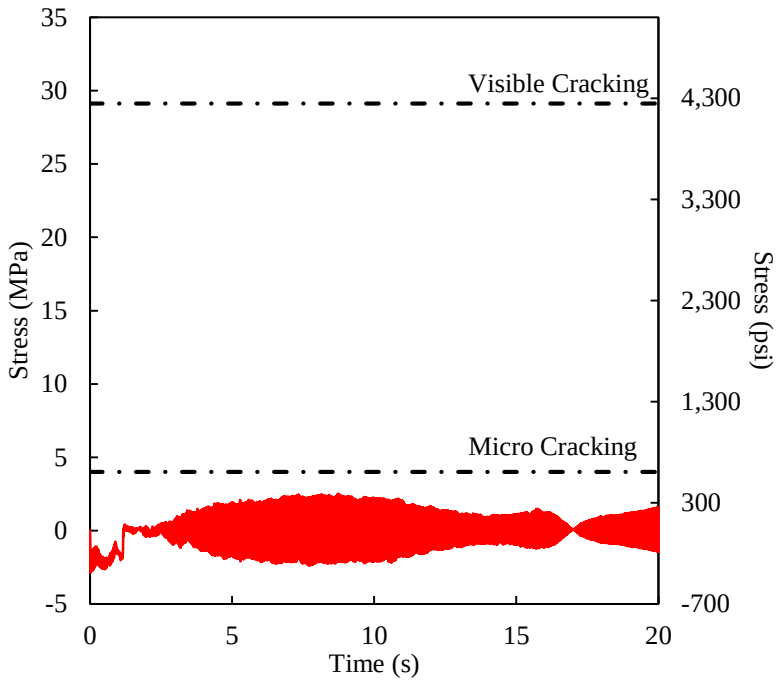

Figure 47: Stress Values for Concrete (Left Column)

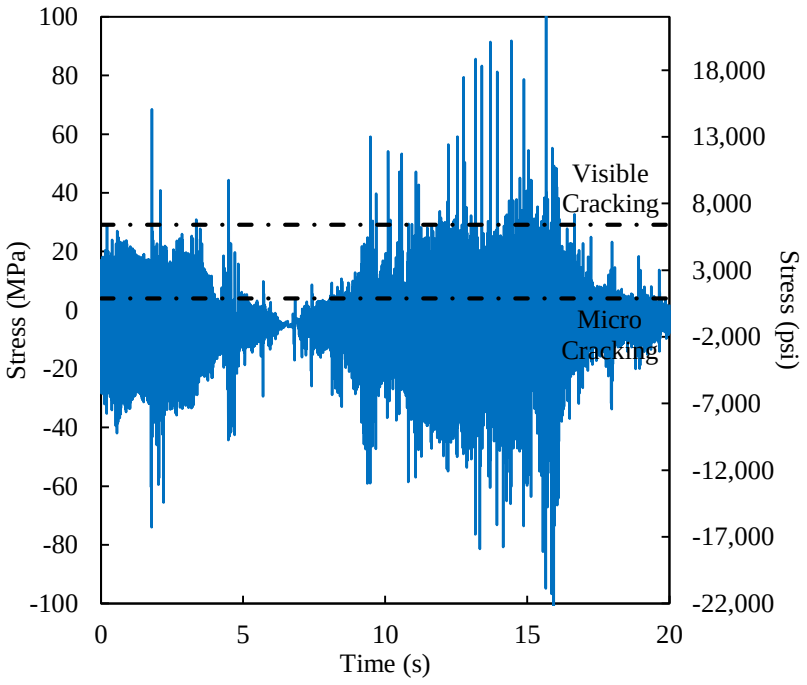

Figure 48: Stress Values for Concrete (Right Column)

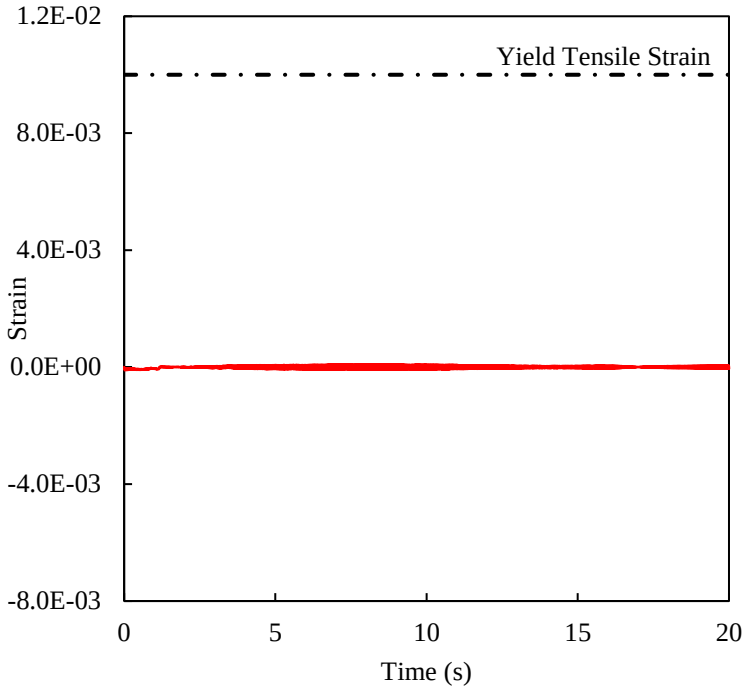

Figure 49: Strain Values for Steel (Left Column)

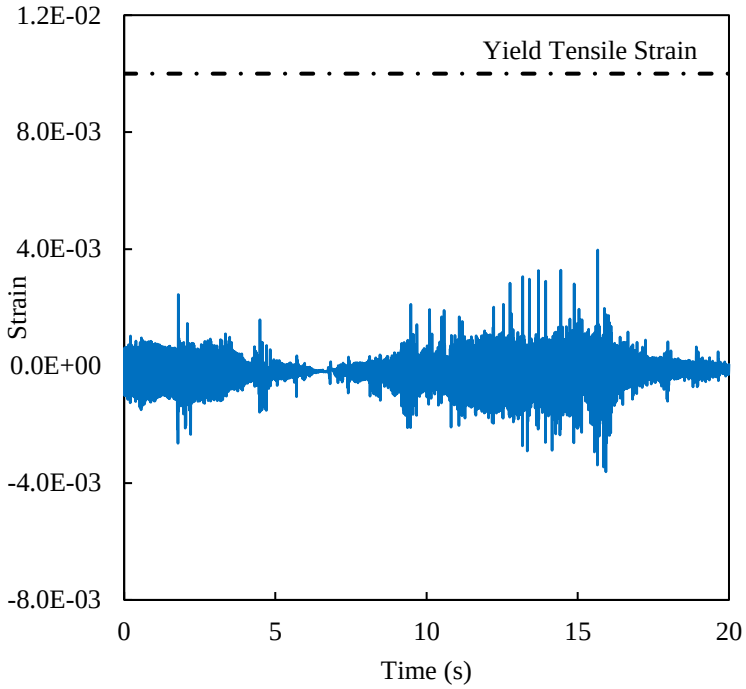

Figure 50: Strain Values for Steel (Right Column)

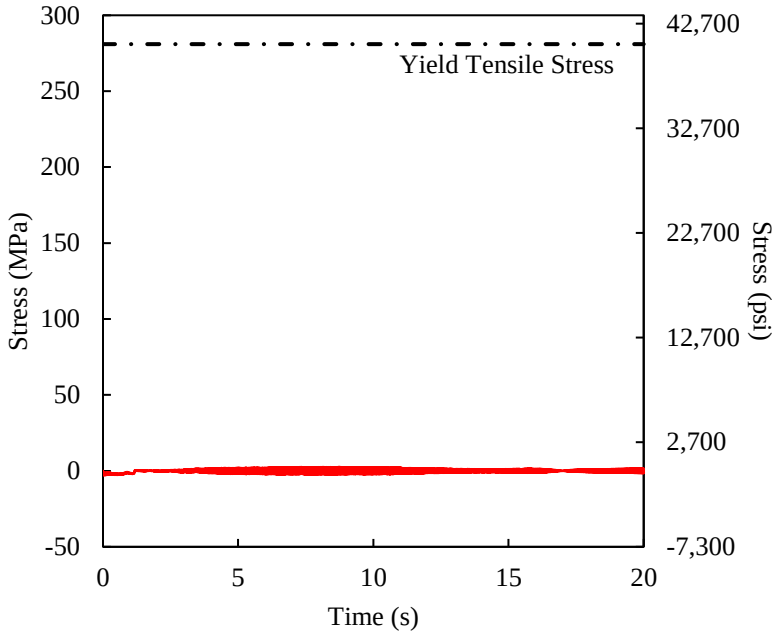

Figure 51: Stress Values for Steel (Left Column)

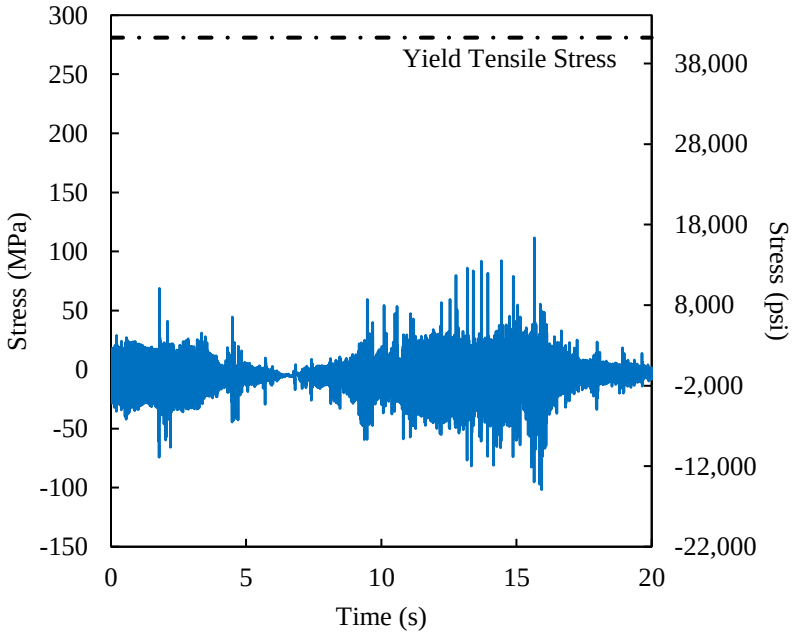

Figure 52: Stress Values for Steel (Right Column)

The recorded data plotted in Figures 46 and 48 shows that the visible cracking limitation of the concrete was exceeded on several occasions. This did not go visually unnoticed. In fact, the concrete frame did show signs of fairly visible cracks and broken

pieces fell loose from the bottom edges of the frame, near the supports. Figures 53 and 54 show the damage sustained by the concrete frame.

Figure 53: Cracks Observed on the Concrete Frame

Figure 54: More Cracks Observed

As for the steel, the results obtained are expected, whereby the yield strain was not reached. The maximum strain and stress values were recorded at around time 17.8 seconds into the test. The values obtained were 0.004 for the strain and 112 MPa (16.3

Ksi). These values are well below the yield limits of 0.01 for the strain and 281 MPa (41 Ksi) for the stress.

Concerning the displacement data, Figure 55 shows the location of the LVDTs installed on the concrete frame prior to testing. Figure 56 draws the displacement profile of the top of the wall with respect to its original position prior to testing.

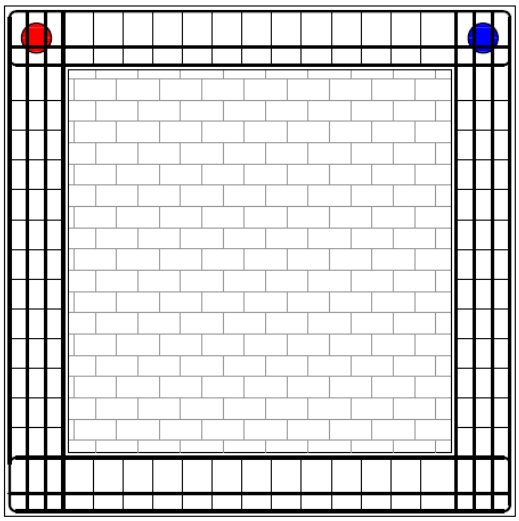

Figure 55: Location of LVDTs on the Wall

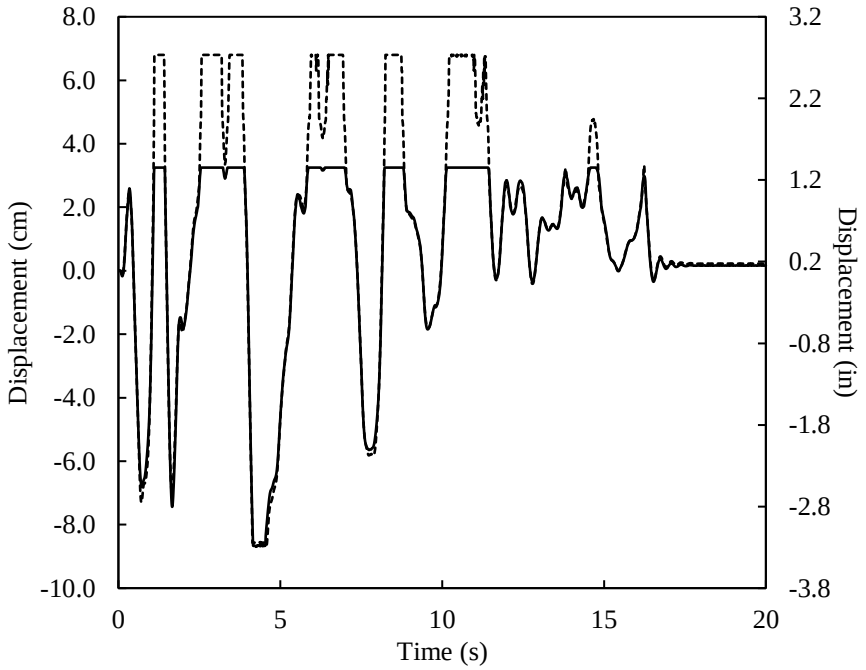

Figure 56: Displacement Data Collected (Both Columns)

The displacement data in Figure 56 shows large differences between the first LVDT and the adjacent one. This discrepancy can be explained by a slight rotation of the frame around its vertical axis, diverging the readings of both LVDTs away from one common value, predominantly in the region where the displacement is positive and the wall bending towards the front.

Results Acquired from SAP2000 Modelling

The concrete frame was also modelled on the finite element analysis software SAP2000. A grid is defined inside the software and the structural members are drawn. The model is constructed by connecting two columns and two beams together to form the square frame. The properties of the reinforced concrete members as determined in the laboratory are assigned to the model. Hinges are assigned as supports for the bottom side of the frame. As for the modelling of the masonry infill wall, Al Chaar [7] strut element is used to connect the bottom joint to its diagonal top counterpart. This strut is modeled using the same properties determined in the laboratory for the masonry material. Equations 4-19 and 4-20 [7] are used to determine the required width of the strut.

$$\lambda_1 = \frac{E_m \times t \times \sin(2 \times \theta)}{4 \times E_c \times I_{col} \times h} \tag{4-19}$$

$$a = 0.175 \times D \times (\lambda_1 \times H)^{-0.4} \tag{4-20}$$

Where λ_1 = strut factor, t = infill thickness, θ = diagonal angle in radians, E_c = modulus of elasticity of concrete, I_{col} = moment of inertia of concrete column, h = infill height, H = column length from center of support to center of support, D = diagonal strut length and a = equivalent strut width.

Figure 57 shows a graphic depiction of the terms found in the previous two equations.

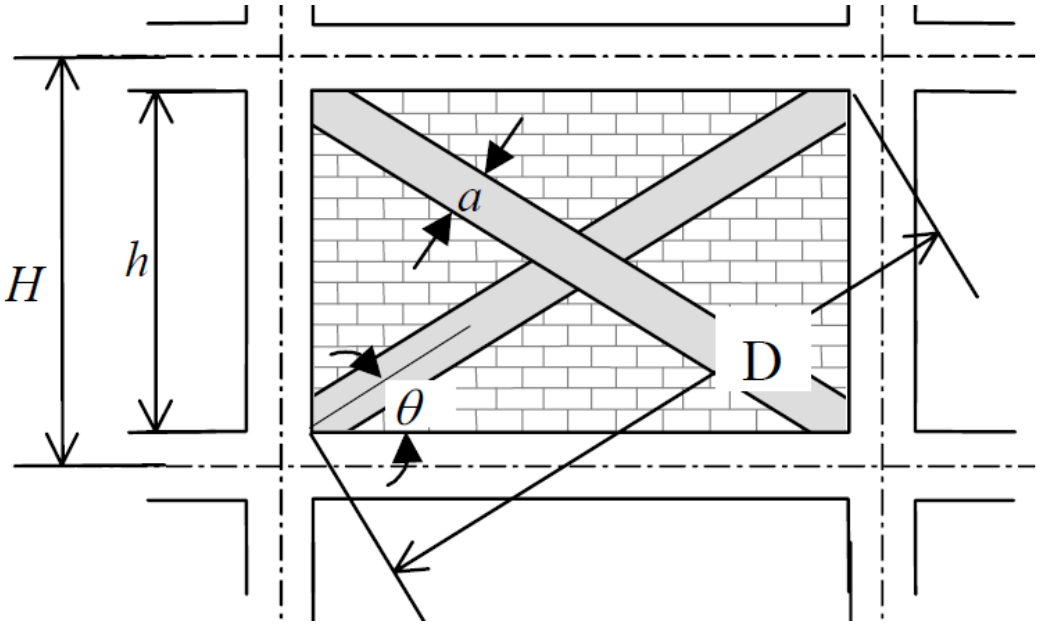

Figure 57: Sketch of a Concrete Frame with Masonry Infill [7]

Equations 4-19 and 4-20 yielded an equivalent strut width for the infill wall of 15.7 cm (6.2 inches). For the connection of the strut to its surrounding frame, two cases were considered. The first involves the assumption that the infill is loosely attached to the concrete frame, dictating the use of hinges to model the connections. In this case, there is no transfer of moment between the structural elements of the frame and the masonry infill wall. The second case assumes that there is perfect bond between the concrete and the frame, therefore dictating the use of fixed connections in the model. In this case, no restriction is applied on the transfer of loads and moments between the strut and the surrounding frame. Figures 58 and 59 illustrate in 3D the two modeling cases, respectively.

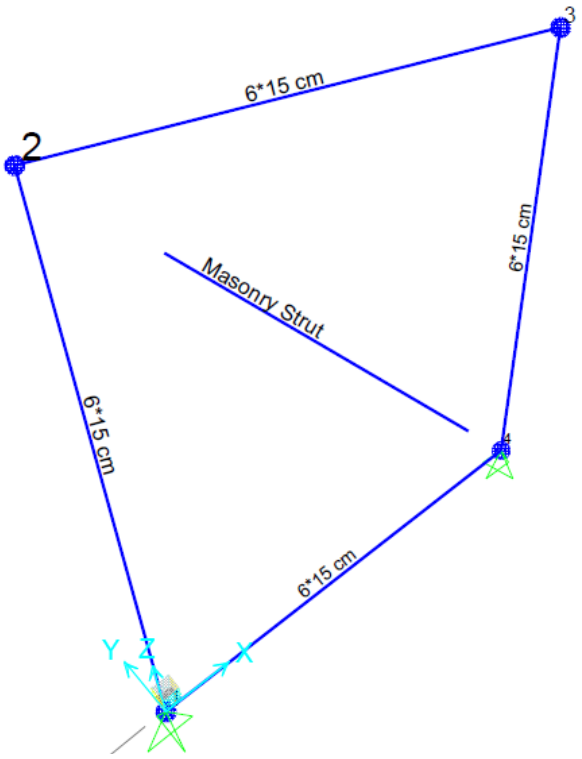

Figure 58: 3D Model with Moment Release

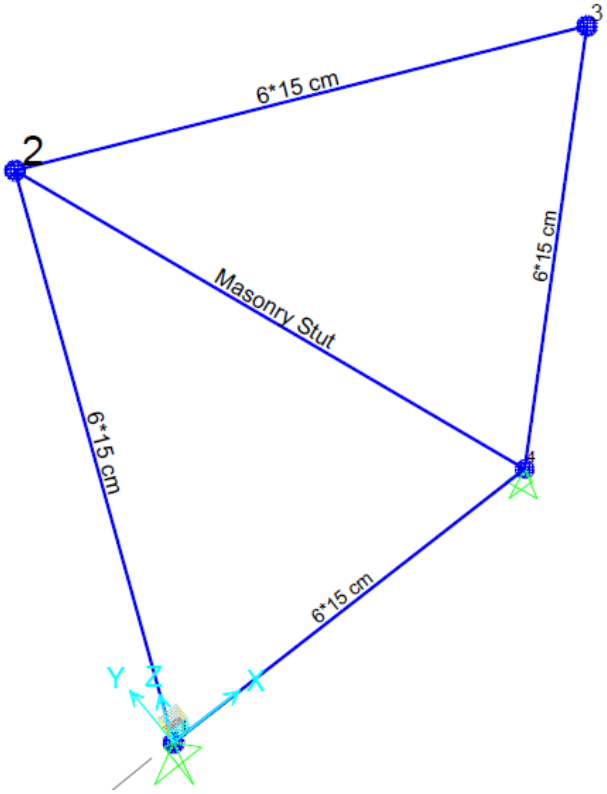

Figure 59: 3D Model with No Moment Release

Two load cases were simulated in SAP2000 in addition to analyzing the MODAL shapes. The first load case includes the self-weight of the structure and the second one includes the non-linear time history assigned to the model. A non-linear time history was defined based on the scaled acceleration data for the El Centro earthquake. The model displacement was not restricted in terms of translation or rotation with respect to the global axes. In other words, the frame is allowed to displace and rotate in all directions.

The model was analyzed and the peak support reactions along with the time of occurrence were recorded. This allows for better comparison between the behavior of the experimental and computer models. Furthermore, the response spectrum of the scaled input is generated along with the base shear in the out-of-plane direction and the displacement at the top joints is compared to the displacement obtained from the experimental tests. In addition, the modes of vibration for this specific frame are generated by the MODAL analysis specific to the SAP2000 program. These modes of vibration are compared to the actual observed and recorded behavior of the frame.

The analysis of both models—the one with moment release and the one with no moment release—shows that the results generated are very similar. Figures 60 and 61 show the negligible difference between both models when the results at the top right corner of the frame are compared. For this reason, the concrete frame with a masonry strut having moment release at the connection points to the frame is adopted and shown. Figures 62 through 67 show the different possible modes of vibration that can occur for this specific wall model. Since no restrictions were applied to the translation or rotation of the model, six modes of vibration were generated. In Figures 60 through 67, the grey color represents the initial model at rest and the blue color portrays the deformed shape.

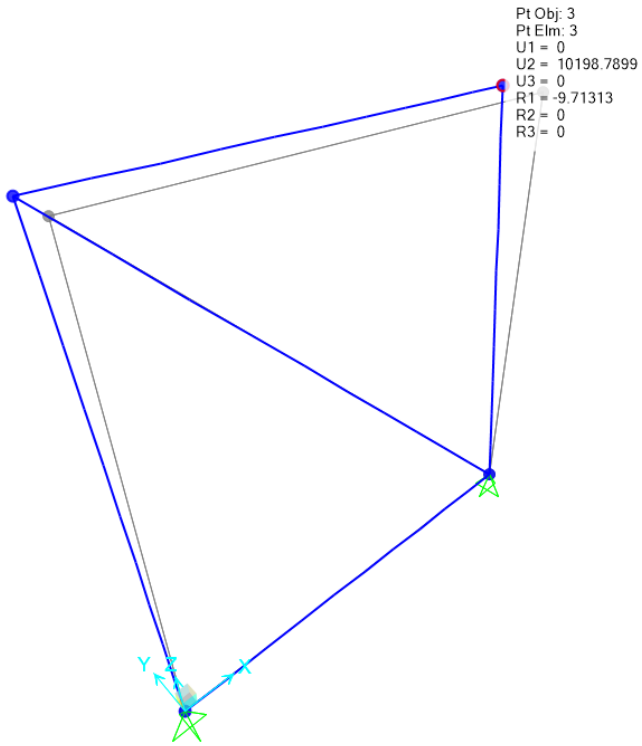

Figure 60: Joint Results for Frame with Moment Release

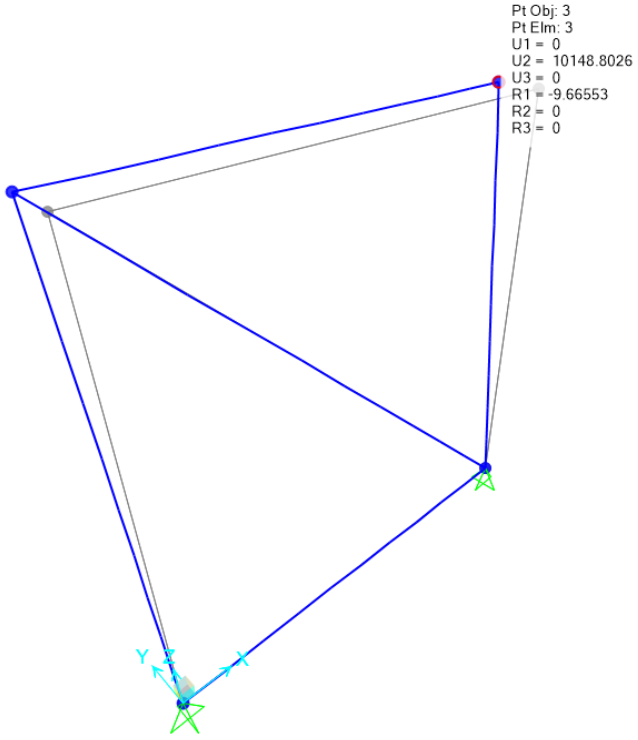

Figure 61: Joint Results for Frame with No Moment Release

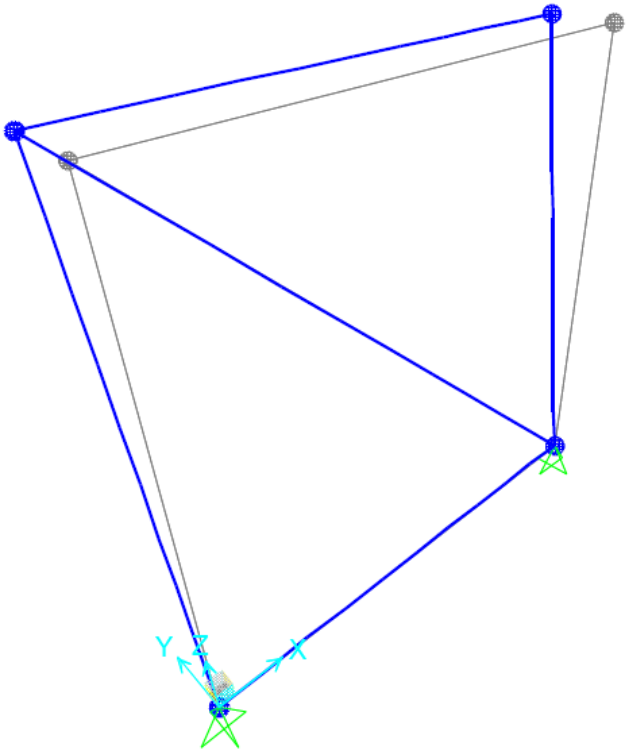

Figure 62: Mode of Vibration Number 1

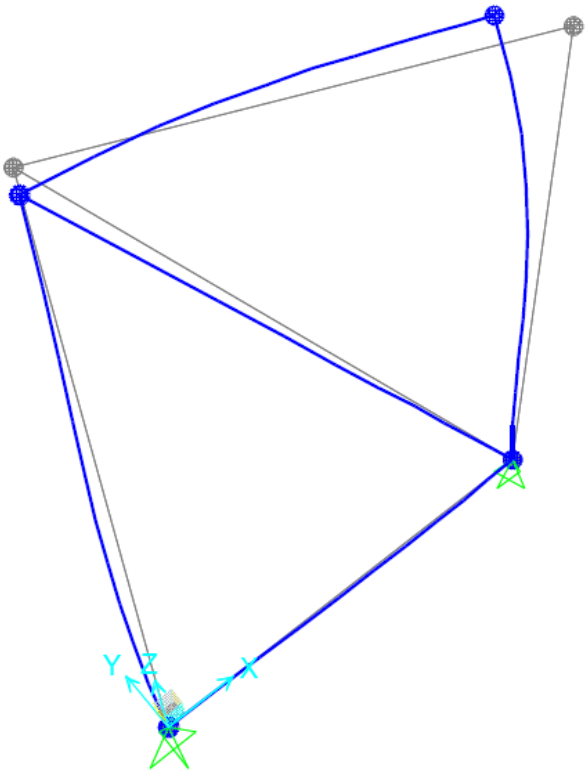

Figure 63: Mode of Vibration Number 2

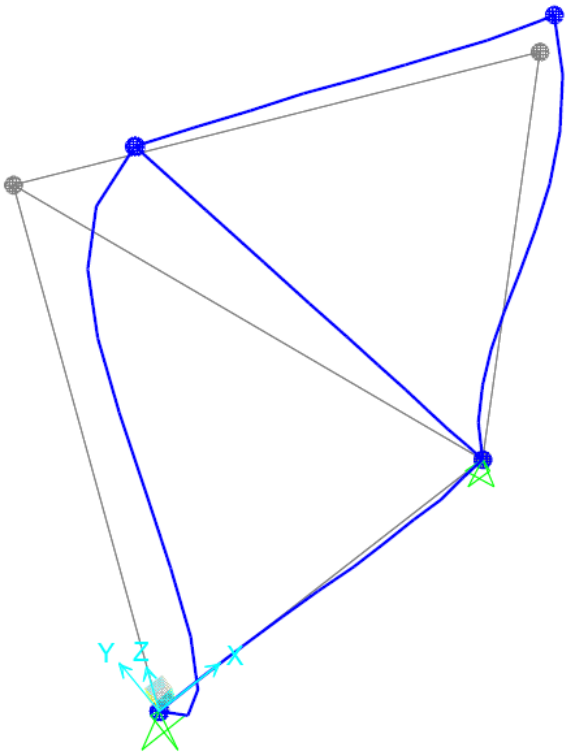

Figure 64: Mode of Vibration Number 3

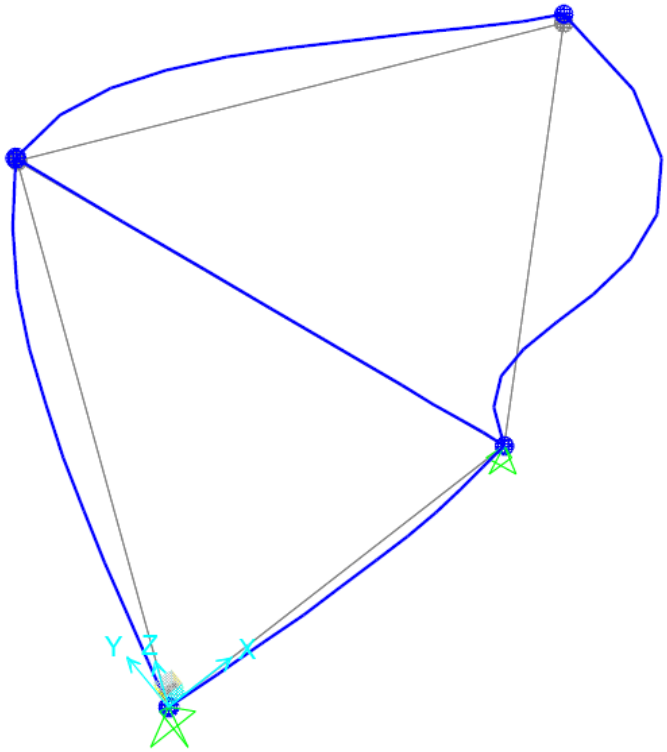

Figure 65: Mode of Vibration Number 4

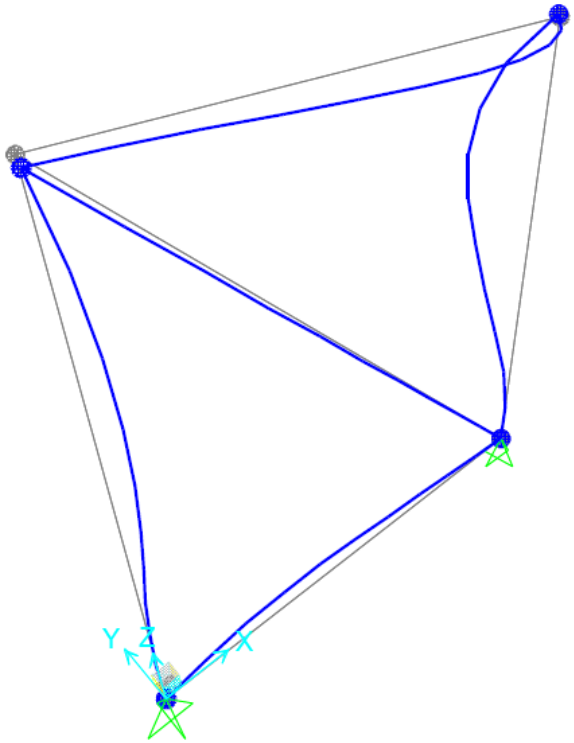

Figure 66: Mode of Vibration Number 5

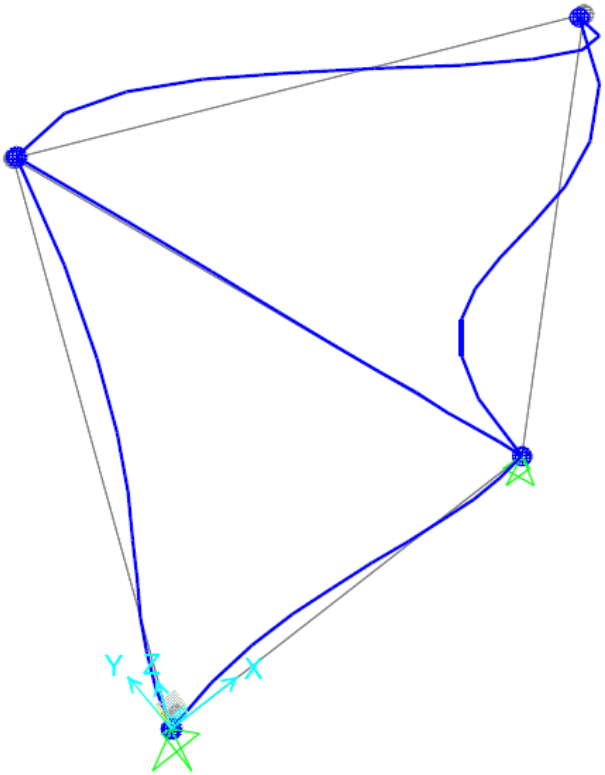

Figure 67: Mode of Vibration Number 6

By inspecting the different modes of vibration, modes Number 1 and 2 were determined to match the observed behavior of the structure during the shake table testing. As previously mentioned concerning Figure 56, the structure experienced translation in the out-of-plane direction (mode Number 1) and a translation and rotation along its vertical axis (mode Number 2). Modes Number 1 and 2 clearly simulate the described behavior. Figure 68 shows the response spectrum of the earthquake generated by the SAP2000 model.

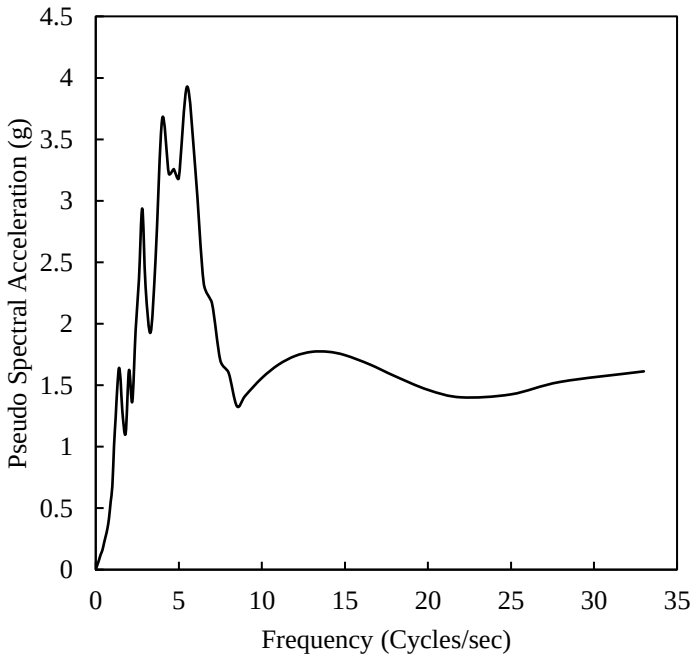

Figure 68: Response Spectrum

The response spectrum generated for the time history function provided as an input in the software is typical with a maximum spectral acceleration of approximately 4g. Figures 69 and 70 show the base shear obtained in the out-of-plane direction and the relevant reactions at maximum displacement.

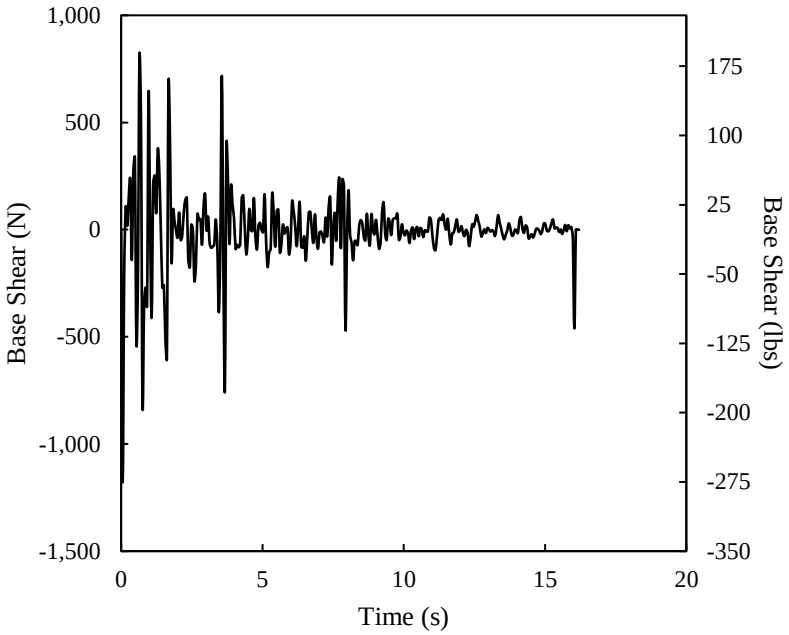

Figure 69: Base Shear in the Out-Of-Plane Direction

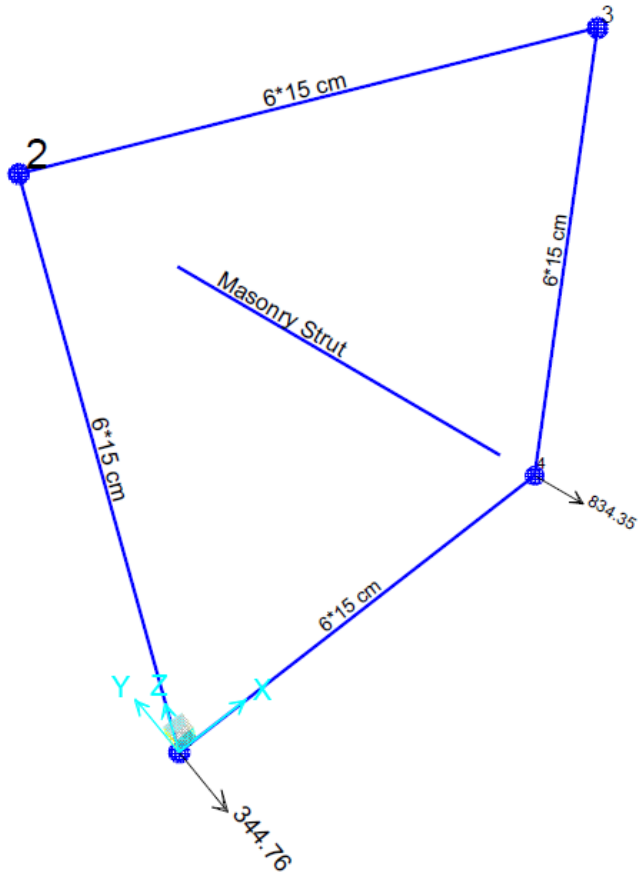

Figure 70: Maximum Reactions at the Supports (in Newtons)

By inspecting Figure 69, the maximum base shear occurring in the out-of-plane direction is found to be approximately 1,200 Newtons (270 lbs.) at 0.054 seconds into the earthquake motion. Figure 70 validates this value of base shear since the sum of the reactions obtained is nearly equal to the base shear obtained from Figure 69. The fact that the reactions are not equal, explains the slight rotation of the frame along its vertical axis, observed during the shake table testing. Figure 71 shows the displacement of the top joints as generated by the software.

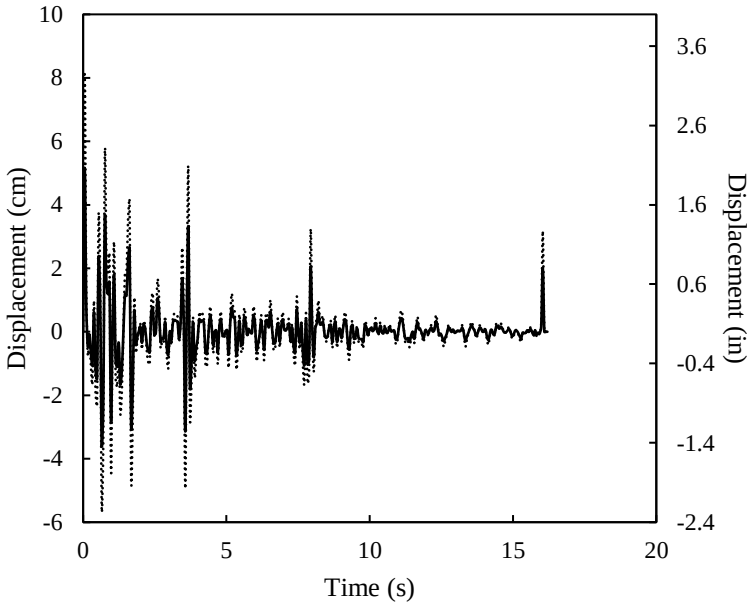

Figure 71: Displacement Chart Generated by SAP2000

It can be seen in Figure 71 that the displacements of the top two joints are not the same, which further explains the rotation of the frame around its vertical axis. In addition, the values obtained by SAP2000 are slightly different and less than the ones recorded by the LVDTs during the shake table testing. The fact that the values recorded experimentally were higher could be attributed to the large weight of the frame applying more rotation on the bearing plate, which could lead to slightly higher displacements at the level of the top beam.

Chapter Five
Conclusion and Recommendations

Unreinforced masonry infill walls are thought to be the most vulnerable structural component in residential and commercial buildings when subject to seismic loading. Design codes recommend that design engineers ignore their structural strength or consider it in a highly conservative manner at best. In the Middle East, their vulnerability arises from the construction practices and the lack of a positive anchorage to their surrounding frame. In fact, previous studies have demonstrated that unreinforced masonry infill walls suffer from a high number of common failure modes including anchor failure, in-plane failure, out-of-plane failure, combined in-plane and out-of-plane failure, and diaphragm related failures. These studies consider structural failure to occur at the onset of cracking.

The aim of this research was to investigate the behavior of unreinforced masonry infill walls under lateral out-of-plane earthquake loads using shake table testing and check the adequacy of infill wall construction techniques widely adopted in the Middle East. Scaled experimental specimens were constructed using the same material properties used in the prototype. The same construction techniques used in residential and commercial projects were adopted in building the specimens. The specimens were tested under out-of-plane seismic loading using factored time history scaled base displacement data from the 1940 El Centro earthquake. Displacement and strain data were recorded and analyzed. Finally, a computer model of the infill wall was developed using SAP2000 software where the masonry infill was modelled as a strut. Comparisons were made between the experimental results and those of the computer model.

Based on the analyzed data obtained from the shake table testing and the results generated by the computer model, the following conclusions are reached:

- For an amplification factor of 2 applied to the scaled base displacement input of the El Centro North South Component, the visible cracking strain limitation of mortar was exceeded in several short instances.
- The mortar joint between the bottom beam of the concrete frame and the first masonry course of the infill wall experienced the highest fluctuations in strains and stresses.
- The concrete frame experienced translation in the out-of-plane direction as well as rotation around its vertical axis.
- Cracks appeared on the surface of the concrete columns and bottom beam and the corners of these structural elements experienced spalling of the concrete.
- The displacement profile generated by the computer model matched the displacement profile obtained by the LVDTs during the shake table testing.
- The modes of vibrations generated by the computer model validated the observed behavior of the concrete frame during the shake table testing.
- The stresses and strains in the concrete columns generated by the computer model did not match the ones obtained during the shake table testing.
- The use of diagonal struts to replace the masonry infill wall seems highly inaccurate in modeling the structural strength of the wall.
- The tensile strength of the mortar bed joints is the governing parameter for the appearance of cracks and their propagation through the masonry infill wall.
- The plastering of the masonry infill seems to have a strengthening effect whereby its presence increased the overall bending strength of the infill.

It is clear from the aforementioned that unreinforced masonry infill walls perform much better under lateral out-of-plane loads than commonly thought. While design codes consider structural failure of these walls to occur at the onset of cracking in the mortar bed joints, the experimental data shows that even when the cracking strain limits have been exceeded, the structural integrity of the infill wall remains intact. It is thus recommended that engineers include infill walls in structural strength calculations of buildings rather than being considered strictly as a dead load.

In any research project and since the scope of work is always predefined, many other questions and insights arise from the moment of developing the literature review to the formulation of certain conclusions. Many of the questions remain unanswered until further research is conducted. The following topics could help better understand the behavior of infill walls related to the Middle East region:

- Development of a complete finite element model to validate the results obtained using shake table testing. This includes modelling the masonry infill as mesh element and assigning it all the obtained experimental material properties.
- Development of a full-scale shake table testing experiment to better simulate the actual behavior of the concrete frames without losing any of the behavioral properties due to scaling problems.
- Development of a shake table testing experiment for a multi-story concrete frame with multiple degrees of freedom.

References

[1] Joseph Plecnik, Thomas Cousins and Edward O'Conner, *Strengthening of Unreinforced Masonry Buildings*, Journal of Structural Engineering, 1986, 112(5), 1070-1087

[2] Roberto Meli and Sergio M. Alcocer, *Implementation of Structural Earthquake-Disaster Mitigation Programs in Developing Countries*, Natural Hazards Review, 2004, 5(1), 29-39

[3] SAP2000 18.1.1, Structural Analysis Program, Computers and Structures, Inc. www.csiamerica.com

[4] Bruneau, M., *State-Of-The-Art Report on Seismic Performance of Unreinforced Masonry Buildings*, Journal of Structural Engineering, 1994, 120(1), 230-251

[5] Bruneau, M., *Seismic Evaluation of Unreinforced Masonry Buildings- A State-of-The-Art Report*, Canadian Journal of Civil Engineering, 1994, 21(3), 512-539

[6] D.E. Allen, J.H. Rainer, *Guidelines for the Seismic Evaluation of Existing Buildings*, Canadian Journal of Civil Engineering, 1995, Vol. 22, No. 3 : pp. 500-505

[7] Abrams, D.P. & Costley, A.C., *Seismic Evaluation of Unreinforced Masonry Buildings*, Eleventh World Conference on Earthquake Engineering, 1996, Paper No. (Vol. 976)

[8] Al-Chaar, G., *Evaluating Strength and Stiffness of Unreinforced Masonry Infill Structures (No. ERDC/CERL-TR-02-1)*, Engineer Research and Development Center Champaign, IL, Construction Engineering Research Lab, 2002

[9] Restrepo-Vélez, L.F., & Magenes, G., *Simplified Procedure for the Seismic Risk Assessment of Unreinforced Masonry Buildings*, Proceedings of the 13th World

Conference on Earthquake Engineering, Vancouver, Canada, 2004, Paper (No. 2561)

[10] Chiou, Y.J., Tzeng, J.C. & Liou, Y.W., *Experimental and Analytical Study of Masonry Infilled Frames*, Journal of Structural Engineering, 1999, 125(10), 1109-1117

[11] Žarnic, R., Gostič, S., Crewe, A.J. & Taylor, C.A., *Shaking Table Tests of 1:4 Reduced-Scale Models of Masonry Infilled Reinforced Concrete Frame Buildings*, Earthquake Engineering & Structural Dynamics, 2001, 30(6), 819-834

[12] Henderson, R.C., Fricke, K.E., Jones, W.D., Beavers, J.E. & Bennett, R.M., *Summary of A Large- and Small-Scale Unreinforced Masonry Infill Test Program*, Journal of Structural Engineering, 2003, 129(12), 1667-1675

[13] Candeias, P., Costa, A.C. & Coelho, E., *Shaking Table Tests of 1:3 Reduced Scale Models of Four Story Unreinforced Masonry Buildings*, Proceedings of the 13th World Conference on Earthquake Engineering, Vancouver, Canada, 2004

[14] Hashemi, A. & Mosalam, K.M., *Shake-Table Experiment on Reinforced Concrete Structure Containing Masonry Infill Wall*, Earthquake Engineering & Structural Dynamics, 2006, 35(14), 1827-1852

[15] Meisl, C.S., Elwood, K.J. & Ventura, C.E., *Shake Table Tests on the Out-of-Plane Response of Unreinforced Masonry Walls*, Canadian Journal of Civil Engineering, 2007, 34(11), 1381-1392

[16] Toranzo, L.A., Restrepo, J.L., Mander, J.B. & Carr, A.J., *Shake-Table Tests of Confined-Masonry Rocking Walls with Supplementary Hysteretic Damping*, Journal of Earthquake Engineering, 2009, 13(6), 882-898

[17] Bothara, J.K., Dhakal, R.P. & Mander, J.B., *Seismic Performance of an Unreinforced Masonry Building: An Experimental Investigation*, Earthquake Engineering & Structural Dynamics, 2010, 39(1), 45-68.

[18] MATLAB and Statistics Toolbox Release 2012b, The MathWorks, Inc., Natick, Massachusetts, United States

[19] R. Pinho, *Shaking Table Testing of RC Walls*, ISET Journal of Earthquake Technology, December 2000, Paper No. 405, Vol. 37, No. 4, pp. 119-142

[20] Daniel P. Abrams, Thomas J. Paulson, *Modeling Earthquake Response of Concrete Masonry Building Structures*, ACI Structural Journal, July-August 1991, Title no. 88-S50

[21] Daniel Abrams, M. EERI, *Effects of Scale and Loading Rate with Tests of Concrete and Masonry Structures*, Earthquake Spectra, 1996, Volume 12, No. 1, February 1996

[22] Satish Kumar, Yoshito Itoh, Kunihiro Saizuka and Tsutomu Usami, *Pseudodynamic Testing of Scaled Models*, Journal of Structural Engineering, April 1997.123:524-526

[23] Harry G. Harris, Gajanan M. Sabnis, *Structural Modeling and Experimental Techniques*, 2nd edition, CRC Press LLC, 1999

[24] Mario E. Rodriguez, M. EERI José I. Restrepo, M.EERI John J. Blandon, *Shaking Table Tests of a Four-Story Miniature Steel Building – Model Validation*, Earthquake Spectra, 2006, Volume 22, No. 3, pages 755-780, August 2006, Earthquake Engineering Research Institute

[25] Miha Tomazevic, *Some Aspects of Experimental Testing of Seismic Behavior of Masonry Walls and Models of Masonry Buildings*, ISET Journal of Earthquake Technology, December 2000, Paper No. 404, Vol. 37, No. 4, pp. 101-117

[26] American Society for Testing and Materials, Designations: *C 494/C 494M Standard Specification for Chemical Admixtures of Concrete, C 39/C 39M Standard Test Method for Compressive Strength of Cylindrical Concrete Specimens, A 615/A 615M Standard Specification for Deformed and Plain Carbon Steel Bars for Concrete Reinforcement, C 109/C 109M Test Method for Compressive Strength of*

Hydraulic Cement Mortars, *C 129 Standard Specification for Nonloadbearing Concrete Masonry Units*, *C1314 Standard Test Method for Compressive Strength of Masonry Prisms*, ASTM International, 100 Barr Harbor Drive, PO Box C700, West Conshohocken, PA 19428-2959, United States, 2011

[27] S. G. Buonopane and R. N. White, *Pseudodynamic Testing of Masonry Infilled Reinforced Concrete Frame*, Journal of Structural Engineering, June 1999.125:578-589

[28] Miha Tomazevic and Tomaz Velechovsky, *Some Aspects of Testing Small-Scale Masonry Building Models on Simple Earthquake Simulators*, Earthquake Engineering and Structural Dynamics, 1992, Vol. 21, 945-963

[29] U.S. Geological Survey and California Geological Survey, *Center for Engineering Strong Motion Data Archives*, accessed January 20, 2015, from USGS website: http://www.strongmotioncenter.org/cgi-bin/CESMD/archive.pl

[30] Daniel J. Velleman, *The Generalized Simpson's Rule*, The American Mathematical Monthly, April 2005, Vol. 112, No.4, pp. 342-350

[31] LabVIEW 2016, National Instruments Corporation, 11500 Mopac Expwy, Austin, Texas, United States

[32] Masood Hajali, Ali Alavinasab and Caesar Abi Shdid, *Effect of the Location of Broken Wire Wraps on the Failure Pressure of Prestressed Concrete Cylinder Pipes*, Structural Concrete, 2015, No.2, pp. 297-303